

Morphology and Formation Mechanisms of Cryovolcanoes in the Solar System

Caroline Liegey

November 22, 2017

Dr. Karen Prestegaard

Dr. Nicholas Schmerr

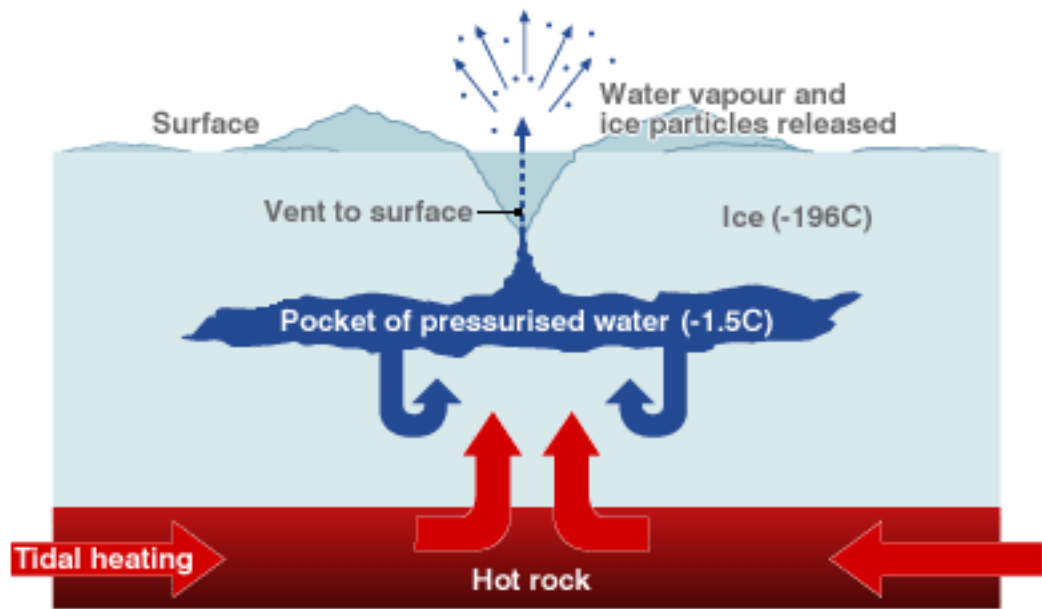
GEOL394

Abstract

Cryovolcanoes are volcanoes that erupt volatile fluids such as water, nitrogen, and methane rather than the silica-based molten rock that erupts on Earth. Cryovolcanic eruptions are rarely observed, therefore eruptive mechanisms are difficult to determine. In this study, I evaluated the morphology of cryovolcanoes and used morphological characteristics to determine flow-type and dome-type volcanic edifices. The cryovolcanoes on Titan and Pluto show morphological similarities with volcanic shield volcanoes built by lava flows on Earth, Mars, and Venus. Therefore, using a laminar flow model for lava flows and constraints provided by the Reynolds number and other equations, I examined possible ranges of flow depth, velocity, and viscosity for cryo-lava flows on Titan and Pluto. Comparison of the cryovolcanoes with Earth and other analogs suggests that cryo-lava flows may have thickness of 100m or more, which is significantly thicker than the Earth average (10 m). Model results suggest that although Pluto and Titan have similar morphologies. However, their different compositions and gravity indicate that Pluto either has a higher flow velocities than Titan, or the cryo-lavas have a lower viscosity, or a combination of the two.

Background

Cryovolcanoes are volcanoes that erupt volatile fluids such as water, nitrogen, and methane rather than the silica-based molten rock that erupts on earth. Their volatile fluids solidify on or near the surface due to low surface temperatures (Lopes et al., 2013). For decades, the concept of a cryovolcano seemed to exist only in the realm of science fiction, the idea that an edifice of solid ice could be created in a similar manner to terrestrial volcanoes did not seem feasible. It was not until six planetary flybys by the Voyager Missions of the four gas giants in our solar system from 1979-1989 that the possibility of a cryovolcano within our solar system became discernable (Kargel, 1994). Voyager found that various satellites show evidence of cryovolcanic resurfacing, and some have terrains strikingly similar to silicate volcano landscapes. Triton and more recently Enceladus display evidence of active cryovolcanism via gas venting that has been observed during flybys. Other satellites such as Miranda, Ariel, Tethys, Dione, Ganymede, and Europa exhibit features consistent with cryovolcanic processes on their surface. In the past decade however, putative cryovolcanic edifices have been discovered on Titan, Ceres, Charon, and Pluto (Witze, 2015).



SOURCE: NASA/JPL/SSI

Figure 1: This figure shows a possible model of cryovolcanism on icy bodies. The diagram illustrates tidal heating melting a portion of the surface ice, creating a cryomagma chamber. The pressurized fluid is vented to the surface through cracks resulting in visible plumes in the moon's southern hemisphere. Image from NASA.

Cryovolcanoes are found on moons and other icy bodies in the outer reaches of the solar system. These volcanic edifices generally occur on planetary bodies beyond the “frost line”, which is the boundary in the solar system where volatile compounds are solid at the low surface temperatures (McCord, 2005). This line occurs in the asteroid belt between Mars and Jupiter (Figure 2). Planetary bodies further from the sun than the frost line are suspected to have active or extinct cryovolcanoes.

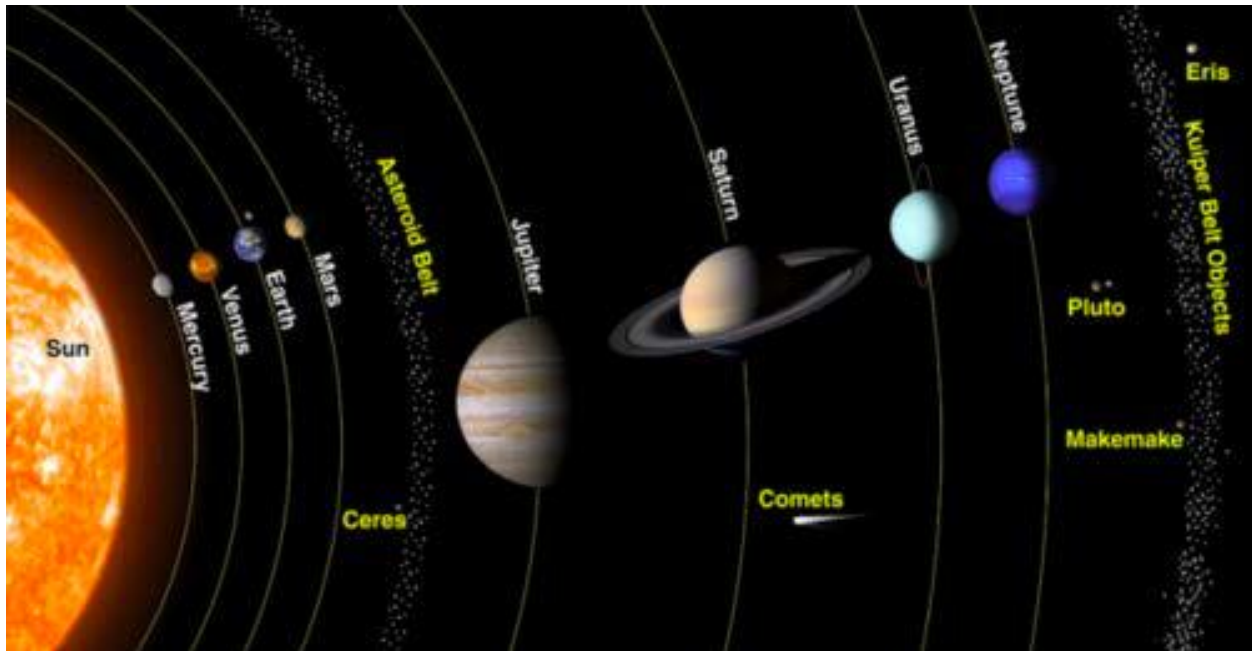


Figure 2: Cartoon of the solar system from SolarStory.net Not to scale.

The mechanism(s) that cause cryovolcanism are a matter of debate, as few cryovolcanoes have been observed during eruptive phases and most have not been confirmed as active. Therefore, the conditions that initiated and supported cryovolcanic activity may no longer be present.

First, for cryovolcanism to occur, a mechanism is required for the generation of heat beneath the surface that forms local pockets of liquid material from melted ices. Secondly, this material must rise to the surface. For icy bodies that have cryovolcanoes, heat generation is primarily thought to be the product of tidal heating (Spencer, 2009). Tidal heat is generated when rotational and orbital energy of the planetary body is dissipated as heat within the interior. This heat must be sufficient to melt or partially melt solids to create a pocket of liquid and possibly gas that rises to the surface. This material may then solidify beneath the surface and form a dome or be vented to the surface forming flows or splatter cones. There are various hypotheses about the mechanisms that cause fluid to move towards the surface. One mechanism is based on density differences, if the melted material is less dense than the surrounding solid ices, the fluid may rise up through the cracks in the denser ice or rise beneath an ice shell, which causes surface doming. Another suggested mechanism is that the fluid is confined under pressure, which will force the fluid up through cracks in the overlying solid material (Steigerwald, 2016). A third suggested mechanism is that the initial heat source that creates this fluid chamber continues to heat the fluid causing convection, which is the driving force that brings it to the surface (Spencer et al., 2009).

The melting temperature, fluid composition, and fluid density of materials in cryovolcanoes are not well constrained, but are important for evaluating cryovolcanic behavior. This brings up the question of what these features are made of and if they act more like a fluid or viscous solid. Visual and infrared spectrometers are used to evaluate the composition of lavas relative to surrounding material, but the exact compositions of lavas and melts beneath cryovolcanoes are hard to determine. As a result, important material properties associated with material composition (e.g. melting point, density, viscosity and freezing temperature), can only

be determined in a relative sense. Properties of possible cryovolcanic magmas can also be estimated based on their compositions. These candidate cryovolcanic magma compositions were estimated by Kargel (1994) and shown in table 1.

Table I: Properties of candidate cryomagmas (eutectic compositions).

Liquid	Liquid Composition, Mass %	Melting Point, K	Liquid Density, g/cm³	Viscosity of Liquid, poise	Solid Composition, Mass %	Solid Density, g/cm³
Water	H_2O 100%	273	1	0.017	H_2O 100%	0.917
Brine	H_2O 81.2% $MgSO_4$ 16% Na_2SO_4 2.8%	268	1.19	0.07	H_2O 50% $MgSO_4$ * $12H_2O$ 44% Na_2SO_4 * $10H_2O$ 6%	1.13
Ammonia-Water	H_2O 67.4% NH_3 32.6%	176	0.946	40	NH_3 * $2H_2O$ 97% NH_3 * H_2O 3%	0.962
Ammonia-Water and non-polar gas	H_2O 67% NH_3 33% CH_4 0.1-2%	176	0.94	40	NH_3 * $2H_2O$ 97% NH_3 * H_2O 3%	0.96
Ammonia-Water-Methanol	H_2O ~47% NH_3 ~23% CH_3OH ~30%	~153	~0.978	~40,000	NH_3 * H_2O ~46% CH_3OH * H_2O ~54%	N/D
Nitrogen-Methane	N_2 86.5% CH_4 13.5%	62	0.783	0.003	N_2 * CH_4 100%	N/D

Data from Kargel (1994)¹.

The instruments of New Horizons contain a near-infrared spectral imager with a linear relation imaging spectral array (LEISA). The instrument analyses the wavelength of light being reflected from the satellite surface, and certain ranges of wavelengths received can be used to estimate a general surface composition. LEISA imaging provides imaging of Pluto at 6 to 7 km/pixel resolution and shows that the surface is comprised of volatile ices (Grundy and Binzel, 2016). Compositional imaging is a similar process with other satellites such as Titan and Ceres as they use similar technology but with varying resolution due to the instruments being different across different missions. Additionally, satellites with significant atmospheres have a greater margin of error in determining composition as the gases in the atmosphere can interfere with the data received from the instrument (McCord and Hansen, 2006).

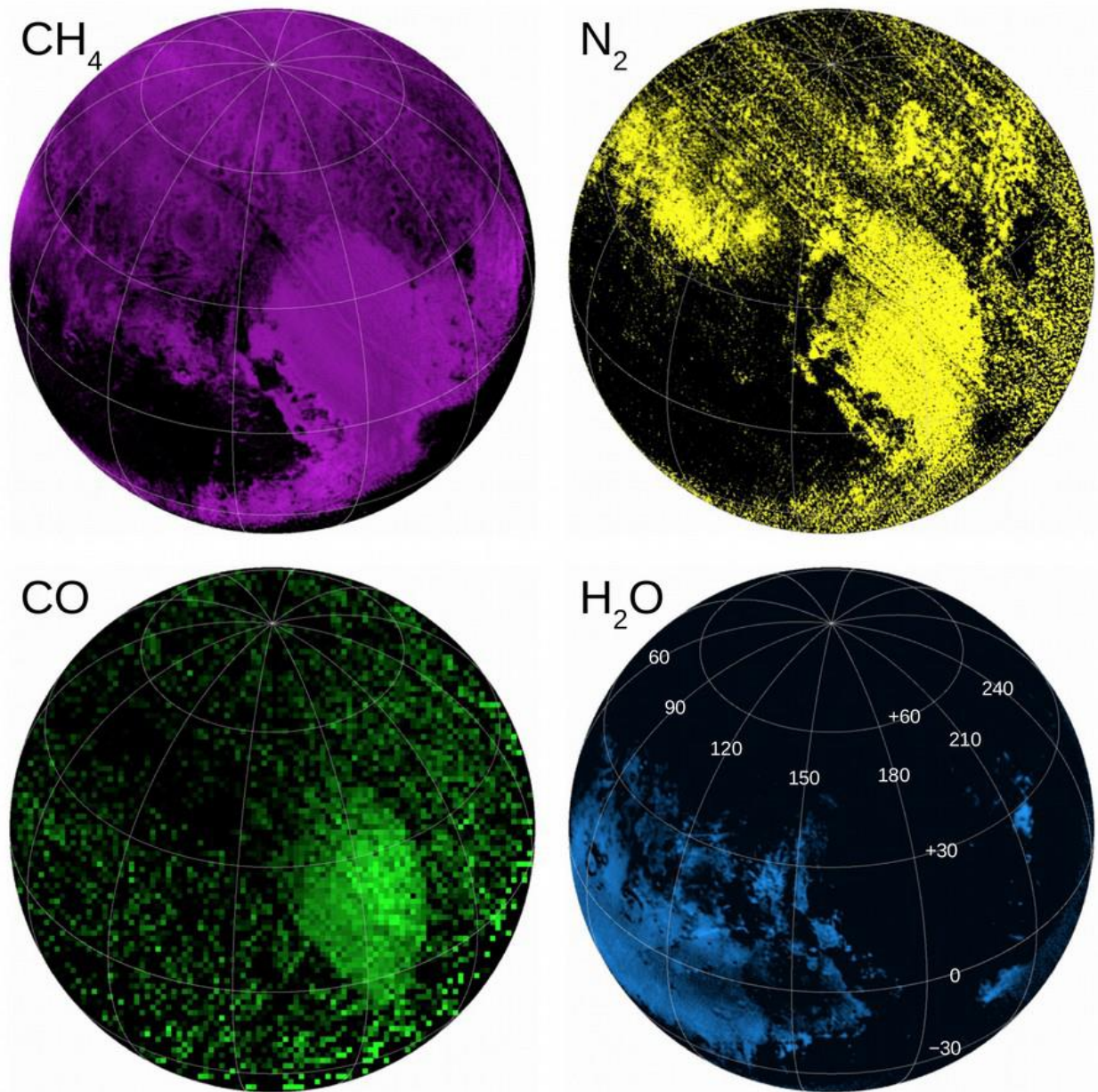


Image I: Pluto compositional imaging indicating areas rich in H_2O , CO , N_2 , and CH_4 . (Grundy and Binzel, 2016)

Table II: Composition and Surface Temperature on Planetary Bodies.

Planetary Body	Composition	Temperature, K	Applicable Eutectoid Composition¹
Ceres ³	Water, salts, and mud	160	Water, Brine
Titan ²	Water and Ammonia	98	Ammonia-Water
Charon ⁴	Ammonia hydrates and water	53	Ammonia-Water
Pluto ⁴	Nitrogen, water, and methane	46	Nitrogen-Methane

Data compiled from (McCord and Sotin, 2006)², (Ruesch et al., 2016)³, and (Desch and Neveu, 2016)⁴.

When comparing the compositions estimated by Kargel (1994) to those derived from spectrometers, the compositions do not exactly align but it does provide a range of values for density, viscosity, and melting temperatures to use. This experiment additionally provides the opportunity to further refine estimates on edifice composition. When testing models of formation with estimated compositions or even compositions with atmospheric interference we can test if the characteristics of the compositions and the resulting topography observed can be tested. If the topographic profile cannot result from the given composition it could indicate that current composition estimates are inaccurate.

As previously mentioned the true composition of cryovolcanic lavas are unknown. However, models can be utilized to determine the range of values for velocity and viscosity to develop a specific aspect ratio as exhibited in Figure 6. These estimates do depend on the density values of Table I, but due to volatile liquids having density values less than 1 g/cm³ this value is well constrained.

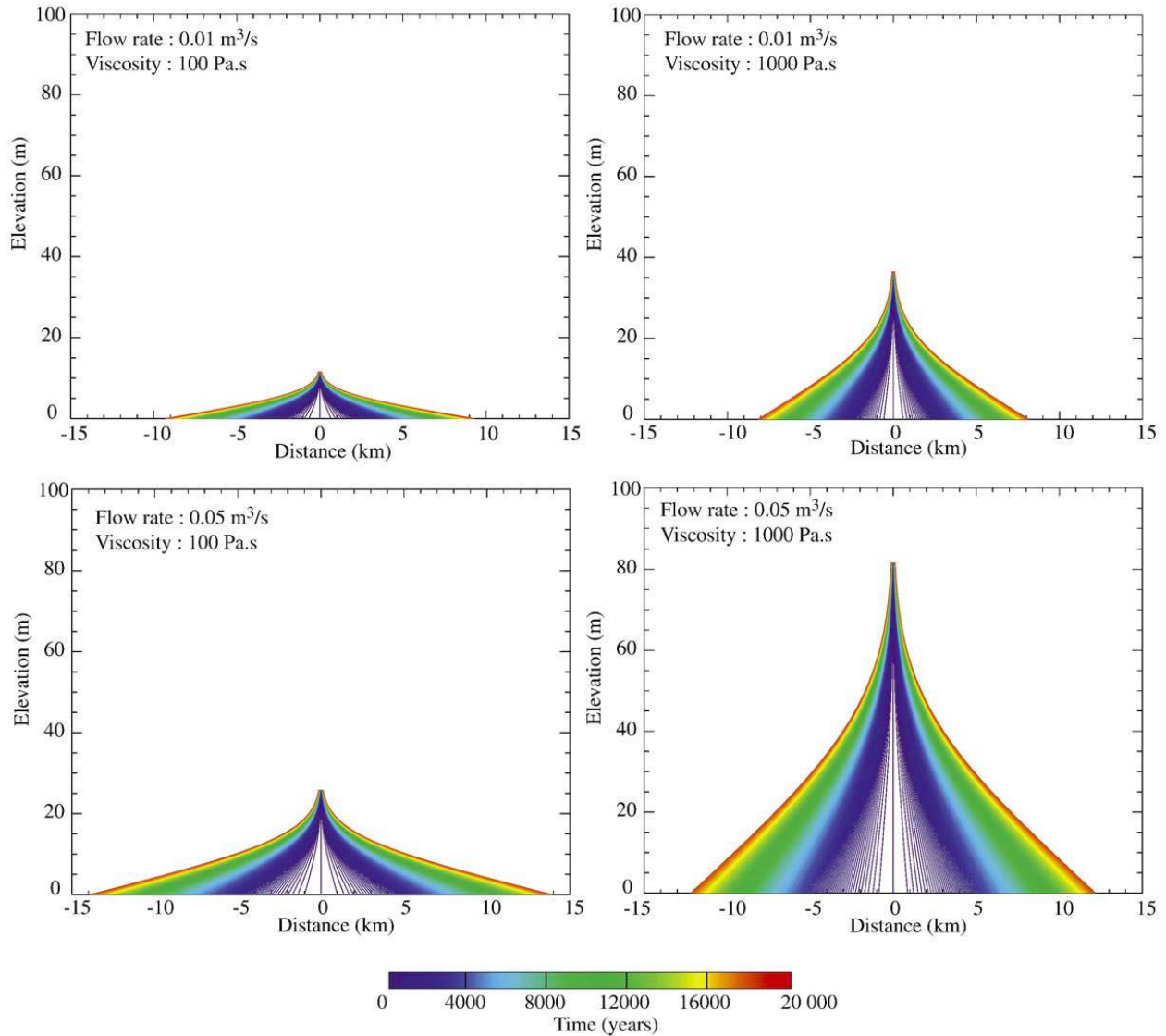


Figure 6: From a Martian shield volcano flow model (Baratoux et al., 2009). This graph exhibits that viscosity and velocity are the main contributors to edifice shape and aspect ratio. Viscosity contributes to edifice height and limits the flow radius. Velocity contributes greatly to flow radius and to a lesser extent edifice height.

Viscosity and velocity, as demonstrated in Figure 6, have a relationship that amplifies or reduces the impact of the other on edifice morphology. They additionally have an inverse relationship to each other when testing the values that could generate a specific morphology. However, the controlling factor of these variables is the composition of the flow.

Research Objectives and Broader Implications

The focus of this research is to examine the morphological features of cryovolcanoes in order to constrain some of the material properties and cryovolcanic processes. Due to there being so few cryovolcanoes whose morphology can be examined at high resolution, insight into relationships between morphology and emplacement materials and processes will also be examined on Earth, Mars, and Venus (Sanchez and Scherbakov, 2012). On Earth, volcanoes built

by flows have different dimensional relationships (e.g. height to radius) than those formed by dome-building. Volcanoes built by flows tend to have lower viscosities than silica-rich magmas that tend to form domes. Therefore, volcano morphology as measured through dimensionless geomorphic and rheological variables of cryovolcanoes on other planetary bodies might provide clues to their formation. Due to the limited information we receive as a result of fly-bys from spacecraft, we must rely on geological features present on the surface to provide insight into past and present geological processes on the observed planetary body (Quick, 2016). Cryovolcanoes specifically can provide insight into thermal and hydrological processes within the planetary body. I expect the results of this research to provide a greater understanding of cryovolcanoes, specifically in regard to their formation mechanisms. Additionally, this research can provide insight into geological processes on icy bodies.

Approach:

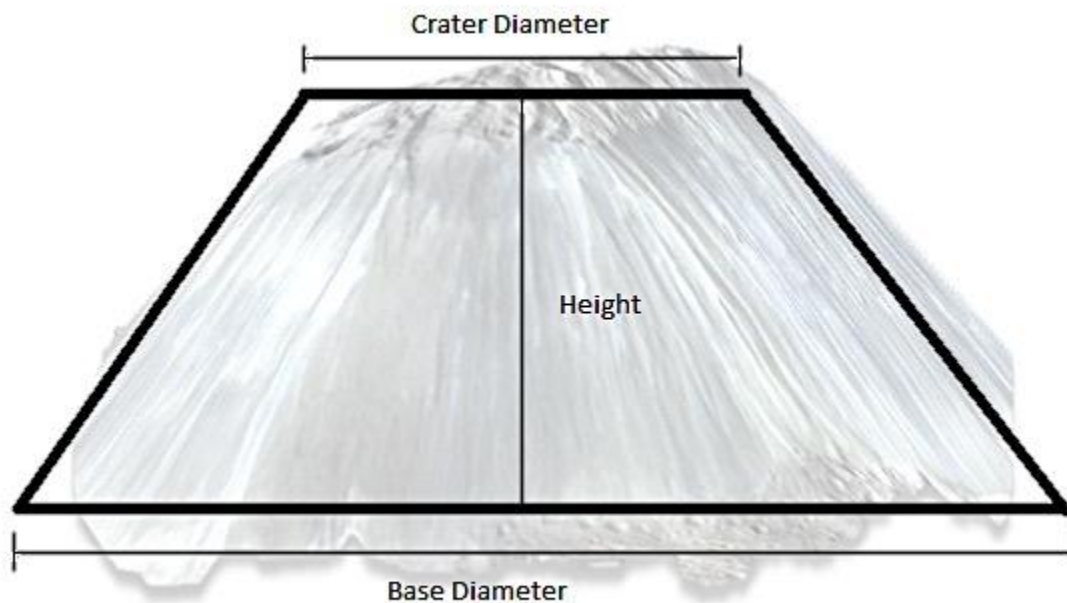



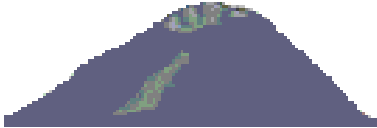


Figure 3: The above figure is a visual representation of cryovolcano dimensions that can be measured.

Volcanoes built by flows tend to have a low height over a significantly larger base width (low aspect ratio). Dome building mechanisms result in a higher height to radius ratio. Additionally, geologic features such as calderas can be indicative of flow formation as only emplacement mechanisms can produce the feature. As a result, volcanic domes will have distinctive cracks at its peak and not have a caldera while volcanoes built by flows can have a caldera (Sanchez and Shcherbakov, 2012). Edifice calderas can further be categorized by the relationship between caldera diameter and base diameter. This can help distinguish between cinder cones and flow domes as cinder cones will have a smaller difference between the diameters in comparison to flow domes.

Another volcano morphology besides shield volcanoes and cinder cones are lava domes, which as previously stated have a higher height to radius ratio. This is due to their formation mechanism as they have significant height build up due to pressure from below that causes surface doming before lava is extruded.

Table III: Volcanic Profiles

Volcanic Profile	Aspect Ratio	Relative Viscosity and Radius
 <p>Shield Volcano</p>	Less than 0.188	Low viscosity and large radius
 <p>Caldera</p>	Less than 0.188	Low viscosity and large radius
 <p>Cinder Cone</p>	Median 0.2	High viscosity and medium radius
 <p>Lava Dome</p>	Greater than 0.2	High viscosity and small radius

Data compiled from (Perez-Lopez, 2010), and Google Earth. Volcanic profile images show the general shape of certain volcanos though they are not to scale. Cinder cones and domes have not been observed with radii over 2 dozen kilometers, but shield volcanoes can span hundreds of kilometers on terrestrial planets.

Although volcano morphology provides clues to magma or cryomagma rheology, dimensionless rheological parameters such as the Reynold's Number, a dimensionless number that measures the ratio of inertial forces to viscous forces, can be used to constrain fluid properties and behavior (Nuclear Power for Everybody, 2017). Previous models of lava flow behavior indicate that velocities, fluid densities, and other flow properties at the lava flow front (which will influence flow travel distances) are consistent with low Reynolds numbers indicative of porous media, laminar flow. Reynold's Numbers are generally categorized into ranges based off of flow behavior. Laminar flows require a Reynold's Number less than 500 and this indicates that the flow moves like a sheet in parallel layers with no disruption between the layers. Values greater than 500 indicate that the flow is transitional to turbulent and that there is a degree of disruption between flow layers. Reynolds numbers greater than 2,000 indicate fully turbulent flow. Applying Reynolds number constrains to flow behavior could be a way to evaluate cryovolcanic emplacement mechanisms.

Hypotheses:

1. Eruptive styles and emplacement mechanisms can be estimated by edifice morphology.
2. A laminar media flow model applies to cryovolcanic flows with Reynold's Numbers <500. The laminar flow model and the Reynolds numbers associated with Earth analogs can be used to constrain the depth, flow rate and viscosity for cryovolcanoes.

Methods:

To achieve my experimental objectives, I will define volcanic morphologies and evaluate contributing factors such as slope, gravity, shear stress, and viscosity. Additionally, I will measure morphologic parameters including physical dimensions and use these morphological measurements to determine whether edifices are more likely flows or domes. Give this decision, I will use analytical models for flow or dome behavior to evaluate emplacement processes.

Table IV: Cryovolcanic Edifices

Satellite	Edifice	Radius, km	Height, km	Density ¹ , g/cm ³	Gravity, m/s ²
Pluto ^{4,5}	Wright Mons	75±0.65	4±0.5	0.783	0.62
Pluto ^{4,5}	Piccard Mons	112.5±0.65	6±0.5	0.783	0.62
Charon ^{4,5}	Kubrick Mons	17±0.4	4±0.5	0.946	0.288
Titan ^{2,6}	Doom Mons	30±3	1.45±0.2	1.13	1.352
Titan ^{2,6}	Erebor Mons	20±3	1±0.2	0.946	1.352
Ceres ³	Ahuna Mons	8.5 ± 0.14	4±0.5	0.946	0.27

Data compiled from (Kargel, 1994)¹, (McCord and Sotin, 2006)², (Ruesch et al., 2016)³, (Stern, 2015)⁵, (USGS, 2012)⁶, and (Desch and Neveu, 2016)⁴.

While there are a few cryovolcanoes on other icy bodies, they do not have sufficient data to test the aforementioned hypotheses. Pluto, Titan, Charon, and Ceres as of now are the only cryovolcanoes with elevation data and the six edifices are the only edifices from these icy bodies to generally be accepted as cryovolcanic in nature. The list of edifices used in this analysis is listed in Table III. The morphology of these edifices will be compared with terrestrial edifices, listed in Table V.

Table V: Edifices of Earth, Mars, and Venus.

Planet	Edifice	Radius, km	Height, km	Density, g/cm ³	Gravity, m/s ²
Earth ⁹	Chaiten, Chile (dome)	1.24	0.34	2.8	9.81
Earth ⁹	Lassen (dome)	4.75	2.34	2.8	9.81
Earth ⁸	Mexican cinder cone	0.38	0.089	2.8	9.81
Earth ⁹	Hawaii (shield)	40	7.5	2.8	9.81
Earth ⁹	Cerro Grande (shield)	8.5	0.68	2.8	9.81
Earth ⁹	Cerro Taciara (shield)	5.5	0.95	2.8	9.81
Earth ⁹	Newberry (shield)	20	2.3	2.8	9.81
Mars ⁹	Olympus Mons	300	22	2.8	3.71
Mars ⁹	Pavonis Mons	187.5	14	2.8	3.71
Mars ⁹	Ascraeus Mons	200	17.4	2.8	3.71
Mars ⁹	Arisa Mons	200	17	2.8	3.71
Mars ⁹	Elysium Mons	120	13.6	2.8	3.71
Mars ⁹	Hecates Mons	90	4.4	2.8	3.71
Mars ⁹	Albor Mons	80	3.8	2.8	3.71
Venus ⁷	Maat Mons	197.5	8	2.8	8.87
Venus ⁷	Sapas Mons	60	1.5	2.8	8.87
Venus ⁷	Sif Mons	150	2	2.8	8.87
Venus ⁷	Gula Mons	200	3.2	2.8	8.87
Venus ⁷	Ushas Mons	250	5	2.8	8.87

Terrestrial data compiled from (de Silva, 2016)⁷, (Perez-Lopez, 2010)⁸ and measurements taken through Google Earth⁹.

Terrestrial analogs were selected based on several criteria. Volcanoes were selected to provide a range of edifice sizes and the reliability of the reported data. Also, isolated volcanoes were selected to avoid the problem with burial or overlapping lava flows. On Earth, multiple volcanoes in the same vicinity obscures the full extent of the volcano radius. Most measurements were compiled from previous studies on these edifices, Mars volcanoes were measured through google earth and selected to reduce error by avoiding overlapping edifices.

Scaling Properties:

Aspect ratio, α , is the slope of the edifice and is calculated by height divided by radius.

$$\alpha = \frac{h}{r} \quad (1)$$

To add credibility to the claim that cryovolcanoes have varying methods of formation, it is important to differentiate the dimensions of the edifice while taking into account other factors. Parameters would vary between the planetary body and even the specific factors at the volcanoes location can be different. For example, surface gravitational constants can be significantly different among the planetary bodies that I examined. Additional factors include temperature, viscosity, and composition. Additionally, these factors are interrelated, for instance temperature affects viscosity as it can change over time as a fluid solidifies. Gravity has the potential to cause

an edifice to deform more rapidly and spread out farther. Thus, it is important to take gravity into account in relation to hillslope gradient.

Other researchers have been able to link morphology to physical processes by comparing known processes on Earth with morphologically similar features on other Planetary bodies. An example of morphological scaling analyses that provides insight into flow processes is the study by Soukhovitskaya and Manga, (2005) to differentiate debris flows from grain flow on Earth and Mars (Figure 5) .

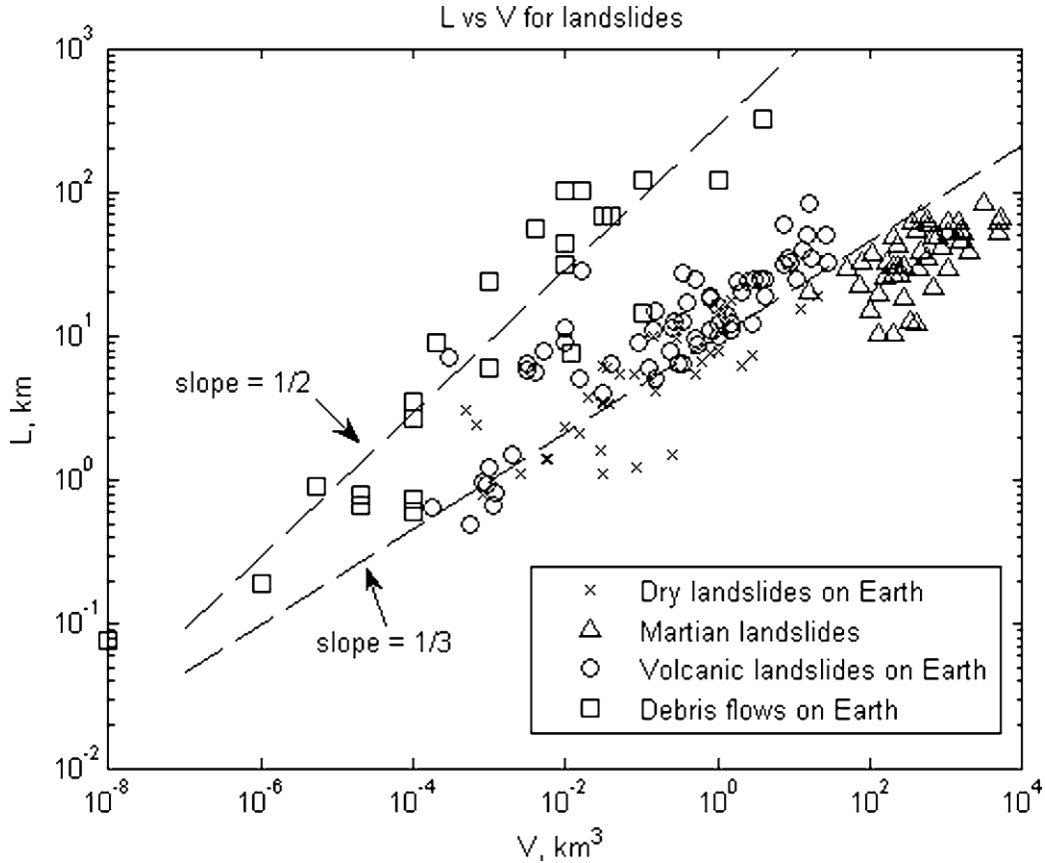


Figure 5: Graph of the volume of a landslide in comparison to their runout length for Martian and terrestrial landslides. From Soukhovitskaya and Manga, (2005).

Soukhovitskaya and Manga (2005) were able to infer flow behavior for Mars by looking at scaling relationships between runout distances and flow volume for both Earth and Mars flows. Similar morphological scaling laws can provide further insight into the properties of cryovolcanoes built by flows and even those with a similar formation mechanism to cinder cones. Additionally, they were able to separate grain flows from debris flows (another type of laminar flow) using the following scaling relationships an analytical model for giant landslides that takes into account energy dissipation, frictional stress, and particle fragmentation:

$$L \sim gV^{\frac{1}{3}} \quad (2)$$

where g is acceleration due to gravity and V is the total volume of the flow, and when calculated would approximately equal the length the flow, L , which would be a similar parameter to cryovolcano radius used in this study. Their second equation (for debris flows) describes a flow with energy dissipation occurs over a thin layer at the base of the flow. In this model, the flow thickens with the travel distance:

$$L \sim g^{\frac{5}{6}} V^{\frac{1}{2}} \quad (3)$$

These equations make the assumption that the flow is the same material which means it is not taking into account the effect of viscosity on flow distance. While these equations may be applicable to cryovolcanoes on the same satellite or volcanoes with similar compositions on different planets (e.g. Earth and Mars); it does not properly express the relationship between cryovolcanoes across various icy bodies due to the difference in compositions (Soukhovitskaya and Manga, 2005). This is supported by cryovolcanoes on Titan and Pluto, which have similar aspect ratios, but different gravities, it shows the opposite length relationship to their real lengths. This indicates that the compositional variations among cryovolcanoes have an important effect on morphology and indicate that viscosity may be a major controlling factor for flows and cinder cones. However, these equations do indicate that there is a scalar relationship between edifice dimensions and rheology. Additionally, these equations open up the use of volume as a variable for flow equations with an assumption that volume can be approximately derived from the volume equation for a cone, with the assumption that the volcano is completely solid. The equation used for the volume of cryovolcanoes is:

$$V = \pi r^2 \frac{h}{3} \quad (4)$$

where r is the radius of the base, and h is the height. Obtaining an approximate volume allows for an approximate calculation of mass based on the density for eutectic compositions (Table I). Potential energy can then be obtained using the calculation of mass and the gravity, g , and height, h :

$$PE = mgh \quad (5)$$

Shear Stress:

While there is a limit in available parameters that are required to describe flows, we do have estimates of variables such as fluid density, slope of volcano, and I can apply this to a range of flow thickness of 10 meters to determine flow shear stress:

$$\text{Flow Shear Stress} = \rho g d \alpha \quad (6)$$

Where ρ equals cryomagma density, g is gravitational acceleration, d is flow depth (which is assumed as 10 meter), and α is gradient. Flows with higher shear stresses are likely flow further, as in edifices with greater gravity and gradient.

Shear stress can then be compared to the basal area, A , of the cryovolcano which can be calculated by its radius, r :

$$A = \pi r^2 \quad (7)$$

Comparison of Dome and Flow Models:

Physical models of emplacement mechanisms have been derived for both dome formation and lava flows. Below I review some of the most recent and commonly used models.

Models of Dome Building:

Models of dome building incorporate material properties into physical models of morphological development. Several models have been developed to describe the formation of volcanic domes on Earth and these models have been applied to topographic analysis of a cryovolcano on Ceres, which can be used to constrain the density and viscosity of the cryogenic magma. The morphology of Ahuna Mons was compared to volcanic domes on Earth with dimensional ratios and overall shape (Ruesch et al., 2016). In that study, they used two previously developed models to analyze volcanic domes on Earth.

The two different models were used to evaluate the topography of Ahuna Mons and compare the topography to theoretical topography of volcanic domes are presented below. The Static Model derives the shape of the dome at static equilibrium between the pressurized magma chamber and the outer rigid carapace of the dome. While an equilibrium equation can be used to model volcanoes, it is making an assumption that the system is at equilibrium which is not in fact the case. The following equations were developed that relate the dome morphology to characteristics of the carapace (thickness and tensile strength) and cryomagma (density):

$$\frac{d(\sin(\phi))}{dr} + \frac{\sin(\phi)}{r} = \frac{\rho g}{\sigma t} \quad (8)$$

where r as the radial coordinate, z is the vertical coordinate, and ϕ the angular coordinate, and

$$\tan(\phi) = \frac{dz}{dr} \quad (9)$$

where t is thickness and σ is tensile strength of the carapace, ρ is the density of the ductile material. The solution to these equations, which describe the shape of the dome, is determined by the following dimensionless parameter that incorporates aspects of the properties of the materials that deform to create a dome (Ruesch et al., 2016). The Static Model is:

$$D = \frac{1}{h} \sqrt{\frac{\sigma t}{\rho g}} \quad (10)$$

where h is the pressure head at the apex of the dome in meters (m), ρ is the density of the magma and it is assumed, g is the gravity of the body, and t is the carapace thickness (meters) and estimated as a range based on the width of the dome and assuming that it is symmetrical, and σ is tensile strength and also assumed to be similar to high viscosity dacite because the tensile strength of water ice is comparable to high viscosity dacite (Petrovic, 2003).

The Dynamic Model is based on a gravity current model for Newtonian fluids and applied to volcanic domes on Earth. The equation gives height, h , and radius, r , as a function of t , time. Unlike the static model, which does not include any changes with time, the dynamic model incorporates the viscosity increase over time (due to cooling) through the parameter θ . The volume, V , is defined as the profile of the static model and is kept constant. This means that spreading does not occur until the entire volume is extruded. Additionally, initial radius, r_0 , is taken arbitrarily between 2 and 6 km (in the case of Ahuna Mons). With this range of values a final kinematic viscosity varies less than 10%. The Dynamic Model is:

$$h(r, t) = \frac{4V}{3\pi r_0^2} \frac{1}{\left(1 + \frac{\theta}{t}\right)^{\frac{1}{4}}} \left[1 - \frac{r^2}{r_0^2} \frac{1}{\left(1 + \frac{\theta}{t}\right)^{\frac{1}{4}}} \right] \quad (11)$$

where the parameter θ is the transformation variable for time dependent viscosity, and is given by:

$$\theta(t) = \Gamma \left(1 - e^{-\frac{t}{\Gamma}} \right) \quad (12)$$

the time dependent viscosity, which provides the value Γ , the time over which viscosity increases exponentially, is:

$$v = v_0 e^{\frac{t}{\Gamma}} \quad (13)$$

where V_0 is the initial bulk kinematic viscosity, and t is time. This equation requires the assumption that the dome does not advance once the relaxation time is met. The time constant, t , is defined by the initial bulk kinematic viscosity:

$$t = \left(\frac{3}{4}\right)^5 \left(\frac{\pi}{V}\right) \frac{3v_0 v_0^8}{g} \quad (14)$$

where g is acceleration due to gravity, and the relaxation time is a variable derived from inferring that the dome stops spreading after a sufficient cooling. An upper limit, t_c , for relaxation time is derived from the consideration that cooling is limited by conduction. For a dome with elevation d , and thermal diffusivity κ , the cooling by conduction timescale is approximated by:

$$t_c \sim \frac{d^2}{\kappa} \quad (15)$$

for a lower estimate, t_r , of relaxation time radiative cooling is used and is assumed that the entire edifice remains isothermal. P is density of edifice material, C_p is heat capacity, T is the temperature during spreading, and σ is the Stefan-Boltzmann constant.

$$t_r \sim \frac{\rho c_p d}{\sigma T^3} \quad (16)$$

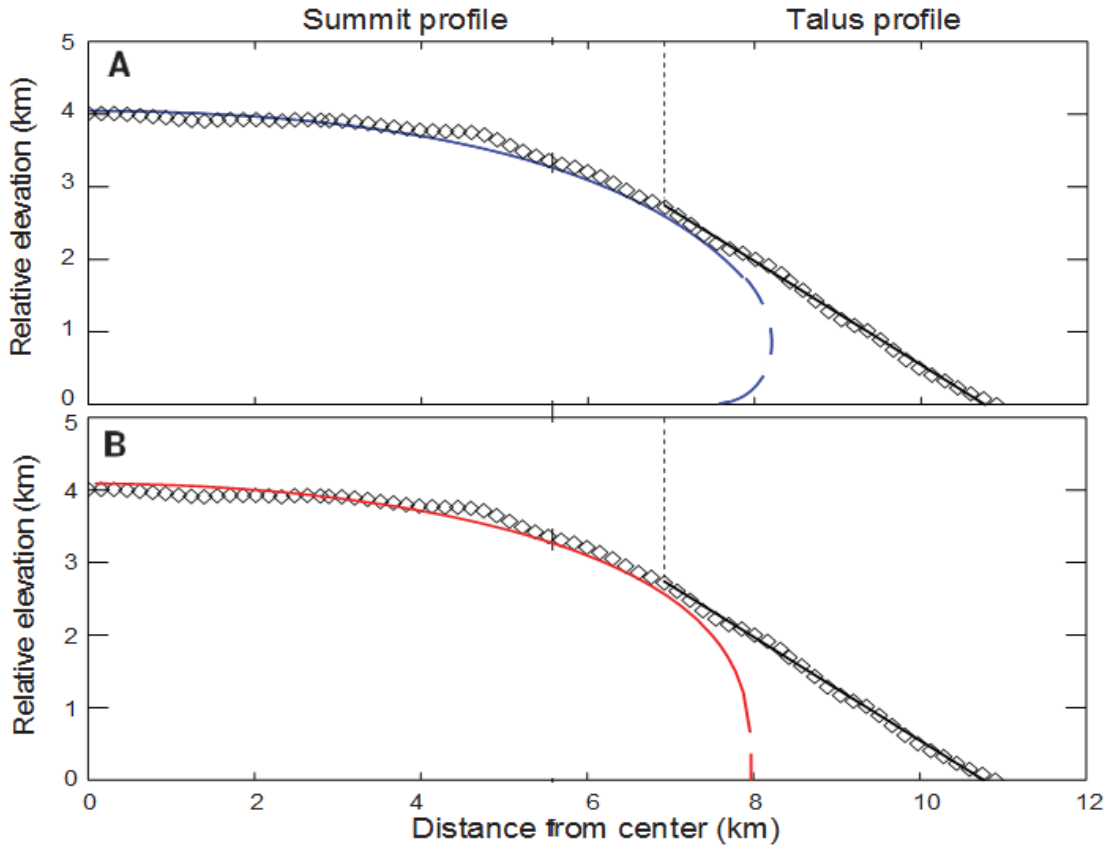


Figure 4: Graph representing the static and dynamic model results for Ahuna Mons on Ceres. The black diamonds show one half Ahuna Mons’ topographic profile as the model can only calculate from the center of the cryovolcano. The blue line shows the profile calculated from the static model and the red line shows the profile derived from the dynamic model. The dashed portions of the lines show where the topographic profile is covered by the talus slope which is represented by the black line. Data and graph from Ruesch et al. (2016).

The experiment conducted by Ruesch et al. demonstrates that Ahuna Mons on Ceres has topography consistent with volcanic domes as displayed in Figure 4.

Model of Lava Flows:

Models of lava flows often include variables dependent on temperature and time. However, these parameters are not known for cryovolcano “lava” compositions. Average surface temperature is known for icy bodies, but the initial temperature of cryomagma upon eruption is unknown. Therefore, I examined a simpler class of models. The model developed by Baratoux et

al. (2009) to model Martian shield volcanoes provides some insight. The model has two similarity variables and it uses height and radius to evaluate the unknown variables of viscosity and velocity at different coordinates along the volcano topography. The similarity equation that depends on height, h is:

$$f = \left[\frac{k\rho g}{\mu Q_0} \right]^{\frac{1}{2}} h \quad (17)$$

where density, ρ , gravity, g , and thermal diffusivity, k , are held constant. Viscosity, μ , and flow rate, Q_0 , are first placed within a range of expected values and then adjusted to better fit the volcano topography coordinates. The second similarity equation:

$$\eta = \left[\frac{\mu}{k\rho g Q_0 t^2} \right]^{\frac{1}{4}} r \quad (18)$$

uses the same constants and variables, but in respect to radius, r , instead of height and with the addition of time, t . These two equations can be used to make a dimensionless equation:

$$f \frac{d^2 f}{d\eta^2} + \left(\frac{df}{d\eta} \right)^2 + \frac{f}{\eta} \frac{df}{d\eta} + \frac{\eta}{2} \frac{df}{d\eta} = 0 \quad (19)$$

which can be solved using a set of boundary equations to obtain a general form $f(\eta)$ of shield volcanoes. However, due to a lack of multiple topographic profiles of cryovolcanoes at a reasonable scale this model can not be directly applied, but the similarity equations can be used, particularly if reasonable bounds for viscosity and velocity can be determined.

Viscosity:

Equations 17 and 18 require reasonable estimates for viscosity and velocity to be determined. To calculate values of viscosity the Jeffery's Equation was used:

$$\mu = \frac{\rho g d^2}{3U} \alpha \quad (20)$$

the value of density, ρ , was chosen for each cryovolcano from the value found on the nearest eutectoid composition on table 1. Gravity, g , and α , which is edifice aspect ratio are both dependent on location. The flow rate, U , was used to determine a maximum and minimum value for viscosity by using maximum and minimum values of flow rate observed on earth (Nichols, 1939). Using those values in the equation will then result in a minimum and maximum for viscosity that can then be used in the Reynold's Number equation.

A dimensionless parameter that describes flow is the Reynolds number:

$$Reynold's\ Number = \frac{\rho U d}{\mu} \quad (21)$$

with ρ being flow material density, U being velocity, d as depth, and μ equaling viscosity. However, we do not know either velocity or viscosity, so this is difficult work with. Assuming the lava flow rate is of the flow front velocity the flows will have Reynolds numbers below 500 (laminar rather than turbulent flow). From this the relationship between flow velocities and fluid viscosity at specific flow depths can be determined.

In this study, I will use edifice morphology to evaluate whether the features are domes or flows. Then I will apply the appropriate physical model to determine flow rheology and other characteristics. For example, if more edifices have morphological characteristics consistent with flows than domes then the flow equations presented above will be utilized to determine viscosity, velocity, and other characteristics will be those previously used to model flows and vice versa.

Results:

Aspect Ratio and Gravity:

Table VI: Cryovolcano Dimensions

Satellite	Edifice	Radius, km	Height, km	Gravity, m/s^2	Aspect Ratio
Pluto	Wright Mons	75 ± 0.65	4 ± 0.5	0.62	0.053
Pluto	Piccard Mons	112.5 ± 0.65	6 ± 0.5	0.62	0.053
Charon	Kubrick Mons	17 ± 0.4	4 ± 0.5	0.288	0.235
Titan	Doom Mons	30 ± 3	1.45 ± 0.2	1.352	0.471
Titan	Erebor Mons	20 ± 3	1 ± 0.2	1.352	0.048
Ceres	Ahuna Mons	8.5 ± 0.14	4 ± 0.5	0.27	0.050

Calculated aspect ratio with data from Table IV.

The relationship between cryovolcano height and radius is plotted from cryovolcanoes on four different planetary bodies. While there are few data on the plot, these data suggest two trends that indicate that Titan and Pluto cryovolcanoes formed by similar mechanisms. The aspect ratios vary from about 0.053 to 0.048, without properly taking into account gravity. Though aspect ratios of shield volcanoes on Earth are around 0.08 this would indicate that based off the hillslope gradient that Pluto and Titan cryovolcanoes and shield volcanoes are similar in that respect. The cryovolcanoes found on Charon and Ceres have much higher aspect ratios at 0.235 and 0.471, respectively. Previous work indicates that Ceres cryovolcanoes have shapes consistent with dome topography.

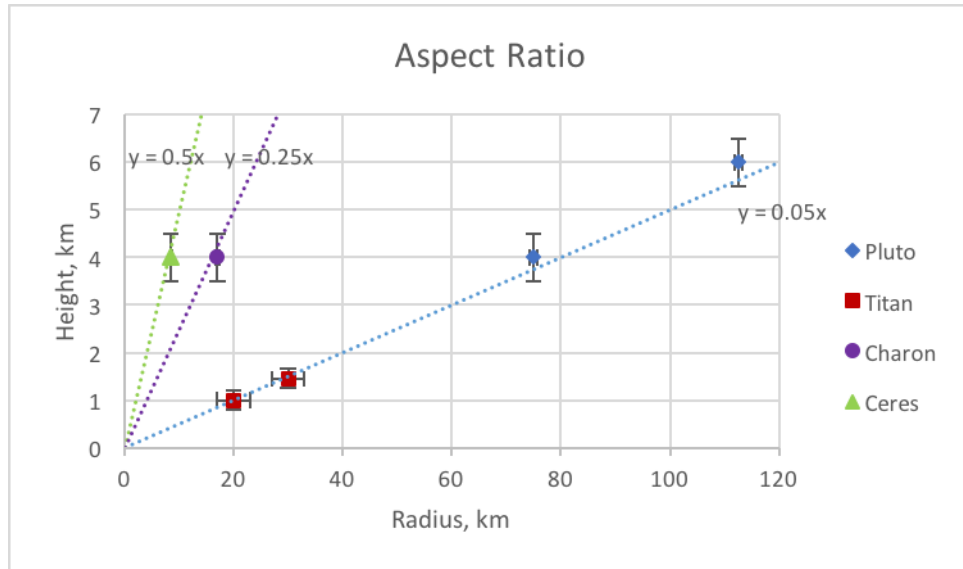


Figure 7: Plot of the radius and height on four planetary bodies. Two trends are evident indicating two different methods of formation based off of hillslope gradient. Due to the exaggerated scale on the y-axis Charon and Ceres appear similar, but their aspect ratios differ. Some horizontal error bars are too small to see on graph. Errors are given by the resolution of each spacecraft and the angular aperture.

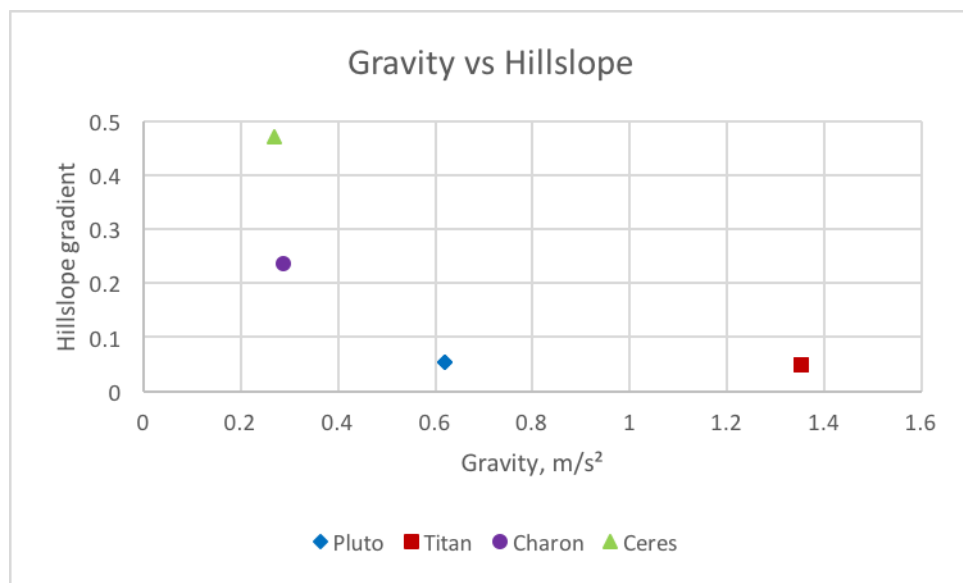


Figure 8: Graph of average hillslope gradient and gravity for each cryovolcano, which indicates two or more populations of volcano type. The two steep volcanoes are found on satellites with low gravity. The four cryovolcanoes with hillslope angles ~ 0.05 have a range of gravitational constants, from 0.6 to 1.35 m/s^2 .

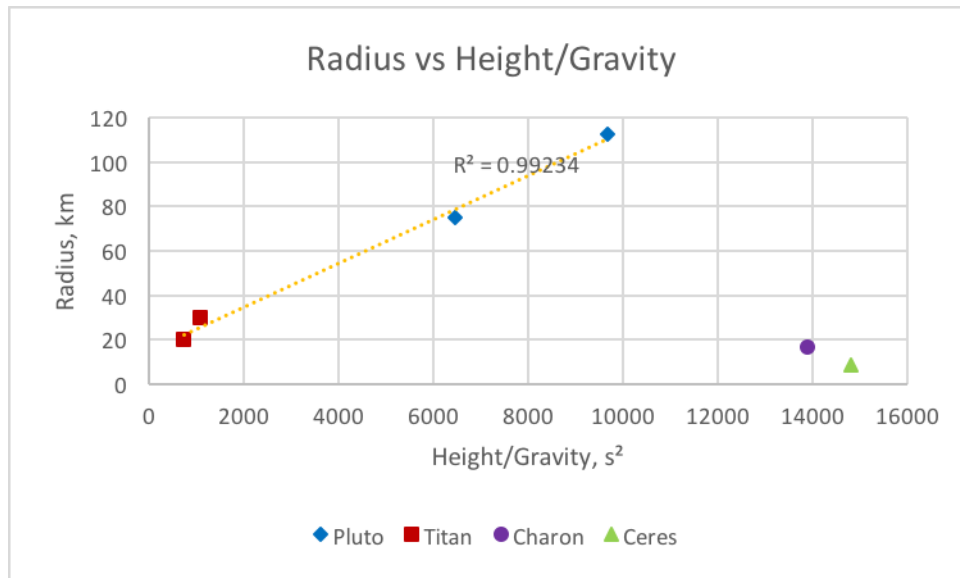


Figure 9: Plot of the radius in relationship to height/gravity. Note that the volcanoes with low aspect ratios have very different characteristics than the two volcanoes with high aspect ratios.

Figure 8. and Figure 9. demonstrates that despite the differences in gravity, particularly between Pluto and Titan, it does not affect the separation of the two trend lines that indicates different formation mechanisms. Figure 9. Specifically plots nearly linearly with an R^2 value of nearly 1 if Charon and Ceres are not included.

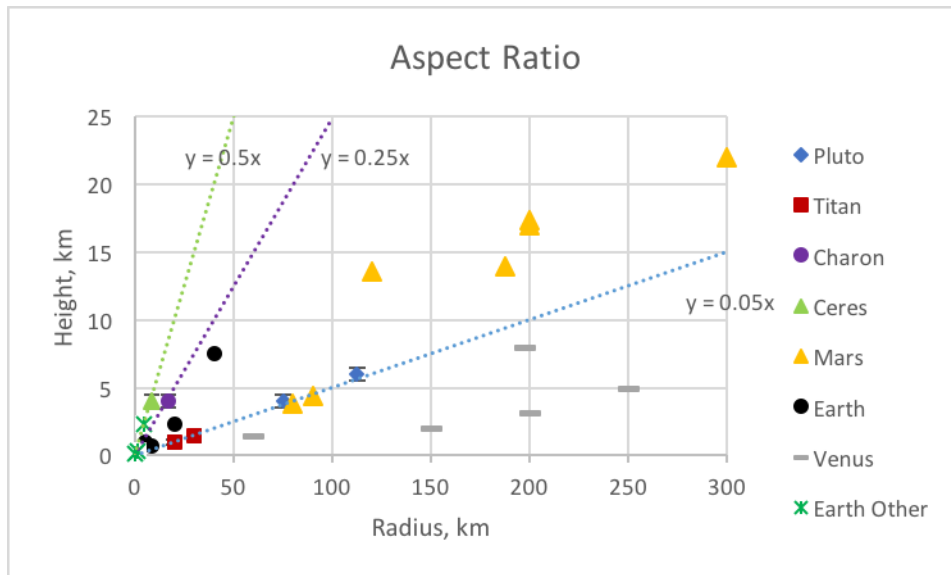


Figure 10: Graph comparing the height to radius of cryovolcanoes with volcanoes found on Earth, Mars, and Venus.

Figure 10 displays that, in relation to aspect ratio, Pluto and Titan volcanoes fall within the range of shield volcanoes on terrestrial planets. Additionally, Ceres also has an aspect ratio consistent with terrestrial domes. However, Charon has an aspect ratio that can fall within the

range of a volcanic dome, but also the range of a cinder cone. Despite the similarities between Ceres and Charon seen in Figure 7, Ceres has an aspect ratio over twice the value of Charon.

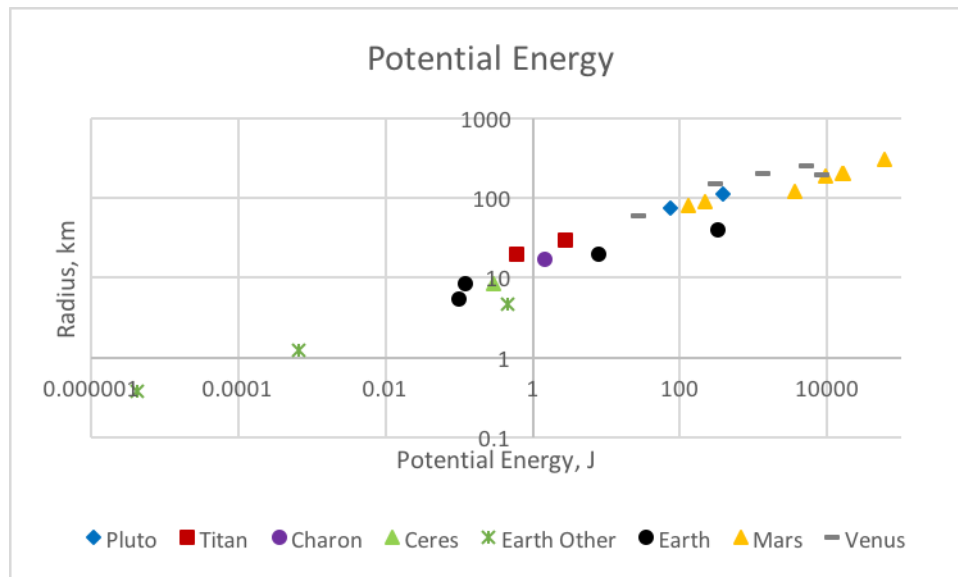


Figure 11: Plot of the radius of six different cryovolcanoes on four different planetary bodies in relation to their potential energy which was calculated by their height, gravity and mass. Mass was derived from density * volume, with volume being calculated assuming a cone shape and the edifice being completely solid. Density was determined from the nearest eutectoid composition density proposed for each satellite seen in Table 1.

In Figure 11, the potential energy in relation to the radius indicate that Titan (red squares) has a larger flow radius than cryovolcanoes on Charon (purple circle) and Ceres (green triangle) that have similar potential energy values. That result is consistent with Charon and Ceres having higher viscosities as they have a lower flow radius for the same potential energy. Pluto (blue squares) has the largest flow radius. The trend of this graph is primarily applicable for cryovolcanoes built by suspected flows. Titan has a gravitational constant that is double that of Pluto, but this graph indicates that Pluto cryovolcanoes have a higher potential energy and flows were able to travel further. Through this graph, initial potential energy can be used as a predictor of the radius of the cryovolcano.

The results of the graphs in this section support hypothesis 1, that eruptive styles and emplacement mechanisms can be determined by edifice morphology. Figures 7 to 9 demonstrate that Titan and Pluto have geomorphology different from Ceres and Charon. Figures 10 and 11 supports that statement by demonstrating that Titan and Pluto are consistent with terrestrial volcanic flows and Charon and Ceres are not.

Shear Stress:

The cryovolcanoes show many morphological and physical characteristics to volcanoes formed by lava flows. The flow laws described in the previous section require parameters that I do not have for the cryovolcanoes. For example, flow depth is not known. However, flow depths are well known on Earth and the average flow depth is about 10 m. Therefore, I compared shear

stress versus volcano radius among the cryovolcano and comparison volcanoes to determine a flow depth that would make the flow behavior similar to the cryovolcano analogs.

Calculations of shear stress for cryovolcanoes at thicknesses, d , of 10 meters, an earth average, does not indicate similarity. This indicates that cryovolcanoes would need to have a significantly larger flow thickness to have similar shear stress and basal area values to terrestrial volcanoes.

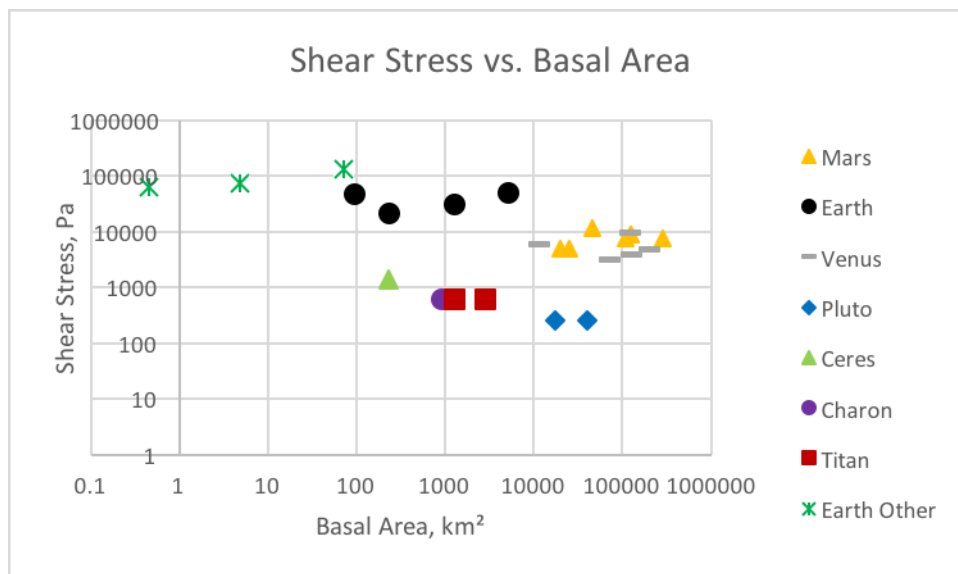


Figure 12: Graph of the relationship between basal area and shear stress of cryovolcanoes and terrestrial volcanoes at a thickness of 10 meters. Note the significantly lower values for the cryovolcanoes.

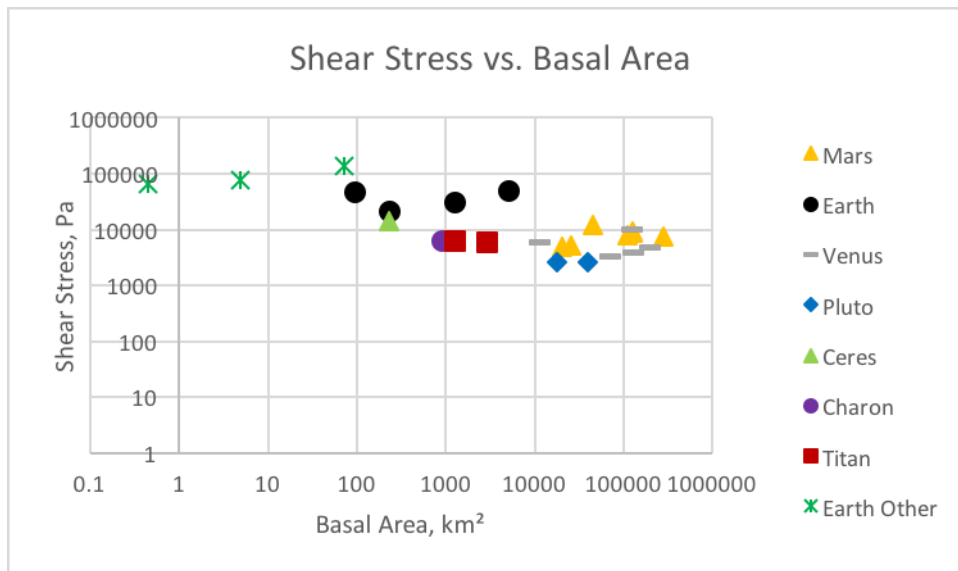


Figure 13: Graph of the shear stress as a function of basal area for cryovolcanoes (at 100m thick) and terrestrial volcanoes (at 10m thick). These data are more similar, suggesting that larger flow thicknesses might be found on cryovolcanoes.

Figure 12 shows that cryovolcanoes would have a significantly lower shear stress than terrestrial volcanoes if they all had the same thickness. The thicknesses of volcanic flows on Earth have been observed to be between 2-30 meters for basaltic flows, but typically around 5-10 meters- which resulted in the constant thickness of terrestrial volcanoes to be chosen as 10 meters (Park and Iversen, 1984).

As a result, to have cryovolcanoes plot similarly to terrestrial volcanoes in relation to their basal area the thickness must be higher. Thus Figure 13 shows the same data as Figure 10, but with the thickness of the cryovolcanic flows being 100 meters, where it falls along the same trend as terrestrial volcanoes. Therefore, it is a possibility that cryovolcanoes have a flow 10 or more times thicker than that of terrestrial flows.

Viscosity:

Due to flows being the more abundant type of cryovolcano based off of their scalar properties, I will use data from Titan and Pluto to model these flows and will compare them to terrestrial shield volcanoes. With thickness established as 10m for terrestrial volcanoes, we can then use the known ranges of flow velocity to calculate the viscosity through the Jeffery's Equation. Since flow rate and viscosity are treated as inversely proportional to each other, determining the range of values for one can constrain values of the other. The fastest observed flow of a basaltic flow front is approximately 2.8 m/s and a commonly used lower bound for lava flow models is 0.01 m/s (Oregon State University, 2017). The range of density is 2.6-3 g/cm³, and for these calculations we assume a constant density of 2.8 g/cm³ (Nichols, 1939). Using these values and each planet's corresponding gravity, we are able to find upper and lower bounds of viscosity and a resulting range of Reynold's Numbers.

Table V: Results- Terrestrial Analogs

Planet	Edifice	Aspect Ratio	Viscosity at 0.01 m/s, Pa s	Viscosity at 2.8 m/s, Pa s	Reynold's # at 0.01m/s	Reynold's # at 2.8 m/s
Earth	Hawaii	0.188	1.67E+07	5.95E+04	<1	1.3
Earth	Cerro Grande	0.080	7.29E+06	2.60E+04	<1	3.0
Earth	Cerro Taciara	0.173	1.54E+07	5.51E+04	<1	1.4
Earth	Newberry	0.115	1.04E+07	3.72E+04	<1	2.1
Mars	Olympus Mons	0.073	2.53E+06	9.03E+03	<1	8.7
Mars	Pavonis Mons	0.075	2.57E+06	9.19E+03	<1	8.5
Mars	Ascraeus Mons	0.087	2.99E+06	1.07E+04	<1	7.3
Mars	Arisa Mons	0.085	2.93E+06	1.05E+04	<1	7.5
Mars	Elysium Mons	0.113	3.88E+06	1.39E+04	<1	5.6
Mars	Hecates Mons	0.049	1.69E+06	6.04E+03	<1	13.0
Mars	Albor Mons	0.048	1.64E+06	5.86E+03	<1	13.4
Venus	Maat Mons	0.041	3.35E+06	1.20E+04	<1	6.6
Venus	Sapas Mons	0.025	2.07E+06	7.39E+03	<1	10.6
Venus	Sif Mons	0.013	1.10E+06	3.94E+03	<1	19.9
Venus	Gula Mons	0.016	1.32E+06	4.73E+03	<1	16.6
Venus	Ushas Mons	0.020	1.66E+06	5.91E+03	<1	13.3

Calculated results from equations 1, 20, and 21 based off of data in Table V.

The calculations for viscosity through the Jeffery's Equation are not the range of possible values of viscosity each edifice could produce, but the viscosity required to generate a volcano with its properties at a specific flow velocity. In reality, the viscosity of basalt is generally accepted to be between 10^3 - 10^6 Pa*s. Other lavas can such as rhyolite are suspected to have viscosities as high as 10^{12} Pa*s (Diniega et al. 2013). From the values derived through the Jeffery's Equation we are able to calculate a range of Reynold's Numbers, which show that terrestrial shield volcanoes fall within the laminar flow range of values.

With the calculations of terrestrial shield volcanoes falling within the expected range of values for the Jeffery's Equation and Reynold's Number, we can then apply the same equations to the cryovolcanoes. First, due to the information that was derived from the shear stress calculations in relation to flow thickness, the viscosity in relation to flow velocity was calculated

at different flow thicknesses. Given that the only cryovolcanoes suspected to be flows are the four on Titan and Pluto due to their aspect ratio, they will be the ones tested.

Thicknesses of 10m, 100m, and 1000m were used to calculate viscosity using the Jeffery's Equation at a range of flow rates from 0.01 to 3.0 m/s. Density was kept constant for each edifice based off of the nearest eutectoid composition found in table I.

Table VI: Cryovolcano Flow Constants

Edifice	Density g/cm ³	Gravity, m/s ²	Aspect Ratio
Wright Mons (Pluto)	0.783	0.62	0.053
Piccard Mons (Pluto)	0.783	0.62	0.053
Doom Mons (Titan)	0.946	1.352	0.048
Erebor Mons (Titan)	0.946	1.352	0.050

Calculated aspect ratio with data based off of Table IV

Due to Wright Mons and Piccard Mons having the same aspect ratio to three significant figures, the above factors that control the variation of viscosity and velocity would be the same and thus generate the same results. This is not to say that the edifices have the exact same viscosity, flow rate, and flow thickness generated these cryovolcanoes, but that the calculable ranges of these values that could have generated an edifice with these specific properties are the same.

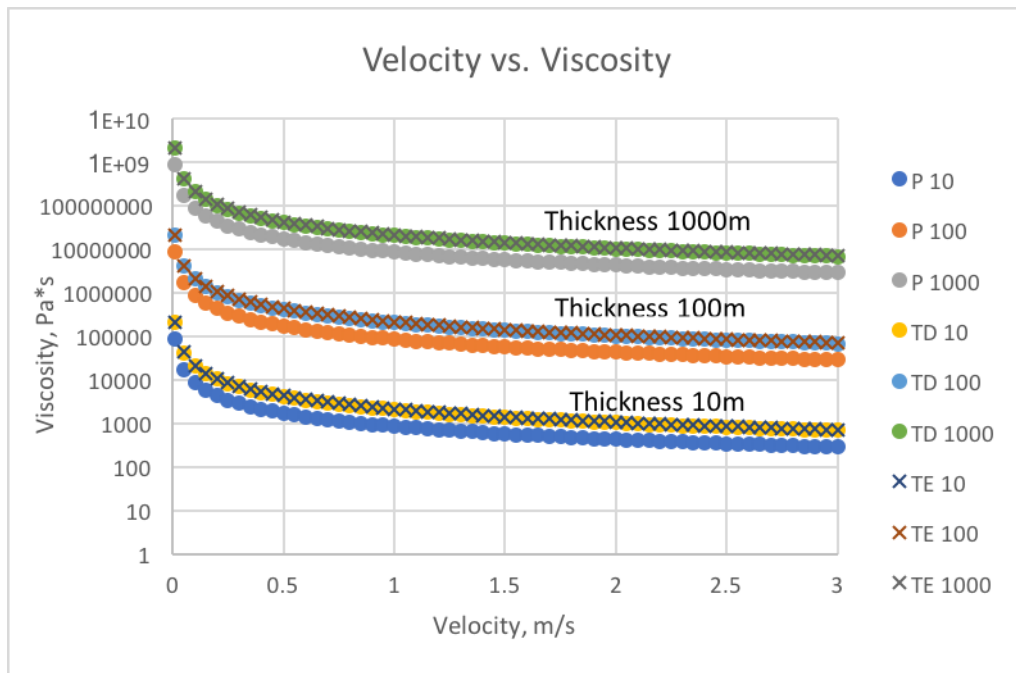


Figure 15: Plot of Titan and Pluto cryovolcanic viscosities for corresponding velocities at thicknesses of 1000 m, 100 m, and 10 m. Calculated using Jeffery's equation.

Figure 15 indicates that the viscosity of cryovolcanoes on Titan have a higher viscosity than those on Pluto for a specific velocity and flow thickness. The three trends shown in the figure are split up by the differences in flow thickness, with 1000 meters having the highest viscosity and 10 meters having the lowest.

Table VII: Results-Cryovolcanic Viscosities and Reynold's Numbers

Edifice	Viscosity, Pa*s (10m)	Viscosity, Pa*s (100m)	Viscosity, Pa*s (1000m)	Reynold's Number (10m)	Reynold's Number (100m)	Reynold's Number (1000m)
Wright Mons	2.86E+02-8.57E+04	2.86E+04-8.57E+06	2.86E+06-8.57E+08	0-82.21	0-8.22	0-0.82
Piccard Mons	2.86E+02-8.57E+04	2.86E+04-8.57E+06	2.86E+06-8.57E+08	0-82.21	0-8.22	0-0.82
Doom Mons	6.82E+02-2.05E+05	6.82E+04-2.05E+07	6.82E+06-2.05E+09	0-41.62	0-4.16	0-0.42
Erebor Mons	7.10E+02-2.13E+05	7.10E+04-2.13E+07	7.10E+06-2.13E+09	0-39.96	0-4.00	0-0.40

Calculated from equations 20 and 21 using data from Table VI and varying thickness.

While Figure 15 displays that Titan has a higher viscosity, this is only generally true if Pluto has the same or higher flow rate. As seen in Table VII, the viscosity for each edifice overlaps with another. The same caveat is applicable to each edifices Reynold's Number; while cryovolcanoes have a larger range of possible Reynold's Numbers on Pluto, it does not mean that the Reynold's Number is higher on Titan. Additionally, the exponential change in viscosity exhibited in Figure 15 at low velocities indicate that those values are improbable. This is due to high viscosities being a characteristic of cinder cones and domes and that the Jeffery's equation accounts for edifice aspect ratio and not edifice size. Meaning that these values of viscosity and velocity can generate an edifice of the same aspect ratio, but not one that has a radius that spans more than several kilometers (Table III).

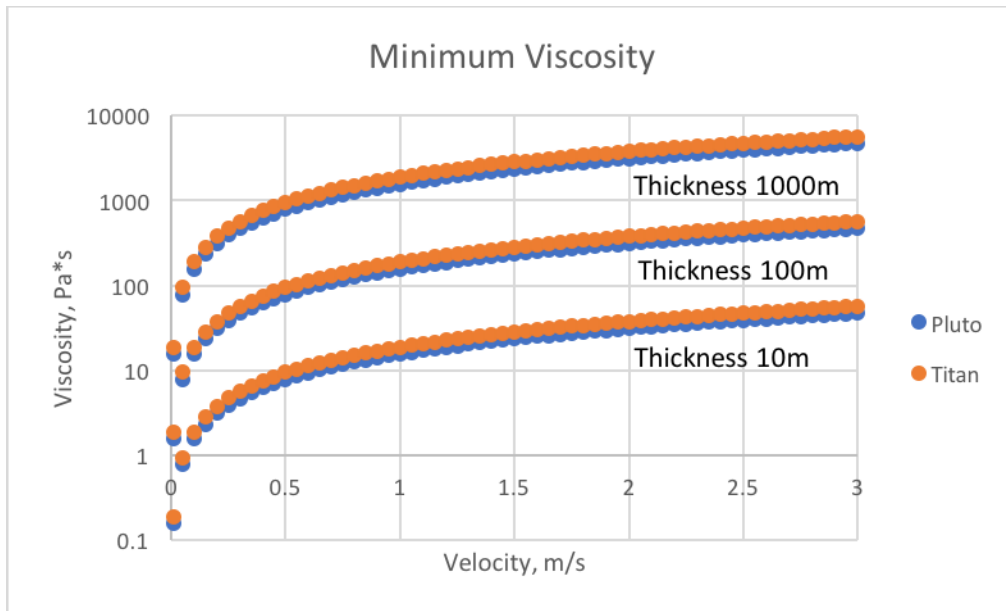


Figure 16: Figure of minimum corresponding viscosity and velocity for flow thicknesses 10m, 100m, and 1000m.

Figure 16 demonstrates the minimum viscosity required for a specific velocity to produce a laminar flow, in other words, to have a Reynold's Number less than 500.

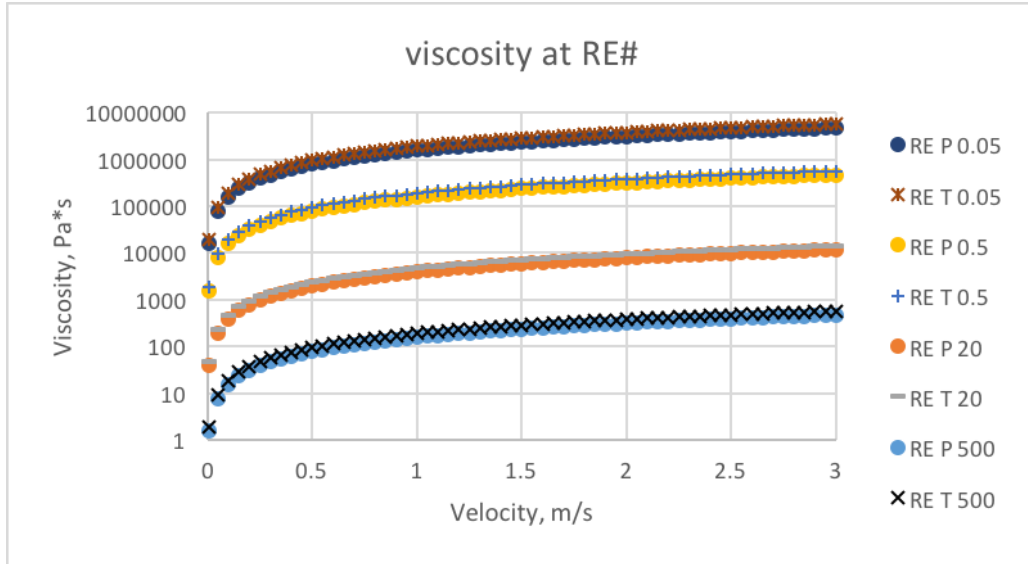


Figure 17: Plot depicting the viscosity in relation to velocity to generate a flow of a specific Reynold's Number for each planetary body at a flow thickness of 100 meters.

Figure 17. exhibits the required viscosity to maintain a specific Reynold's Number for each satellite. This graph continues to show that Titan has a higher viscosity than Pluto to maintain a specific Reynold's number over a range of velocities. Additionally, lower Reynold's Numbers require a higher viscosity for the same velocity.

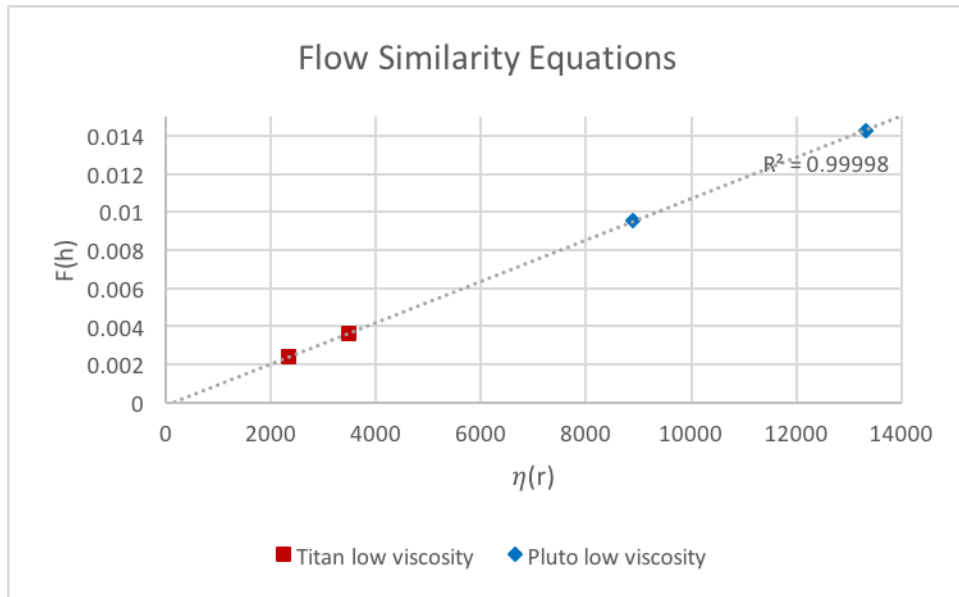


Figure 18: Plot of similarity equations 17 and 18 using the calculated viscosity lower bound in Table VII and maximum velocity of 3 m/s for Titan and Pluto. Values of thermal diffusivity and time were set at constants of $10\text{E}-06$ and $10\text{E}+07$, respectively. Exhibits R^2 value of 0.99998.

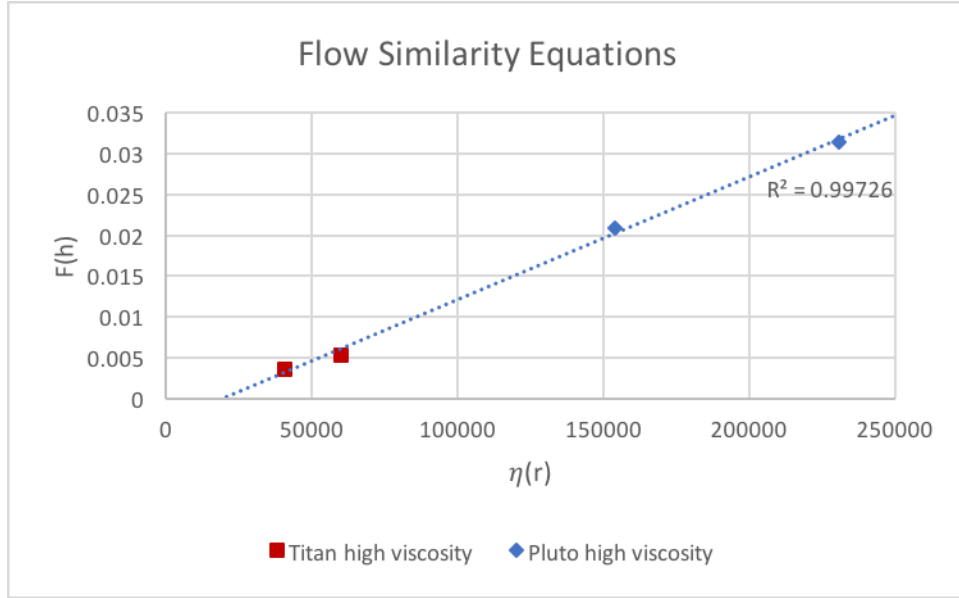


Figure 19: Plot of similarity equations 17 and 18 using calculated viscosity upper bound in Table VII and minimum velocity of 0.01 m/s for Titan and Pluto. Values of thermal diffusivity and time were set at constants of 10E-06 and 10E+07, respectively. Exhibits R^2 value of 0.99726.

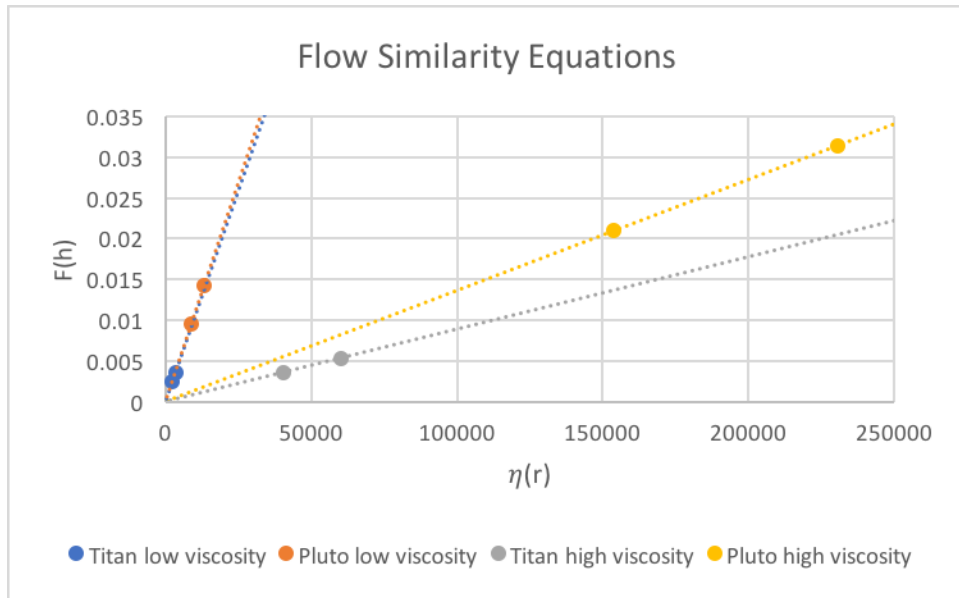


Figure 20: Graph displaying combined data of Figure 18 and 19 with separate trend lines for each data set.

Figures 18 to 20 support that Titan and Pluto cryovolcanoes are built by flows due to the trends mirroring those seen in Figure 7 for aspect ratio. The differences in R^2 value between the upper and lower bounds of viscosity observed in Figures 18 and 19 indicate that the low viscosity and high velocity values are closer to the true values of these variables. This is due to the R^2 value for the high viscosity and low velocity being further from one than the R^2 value of the aspect ratios.

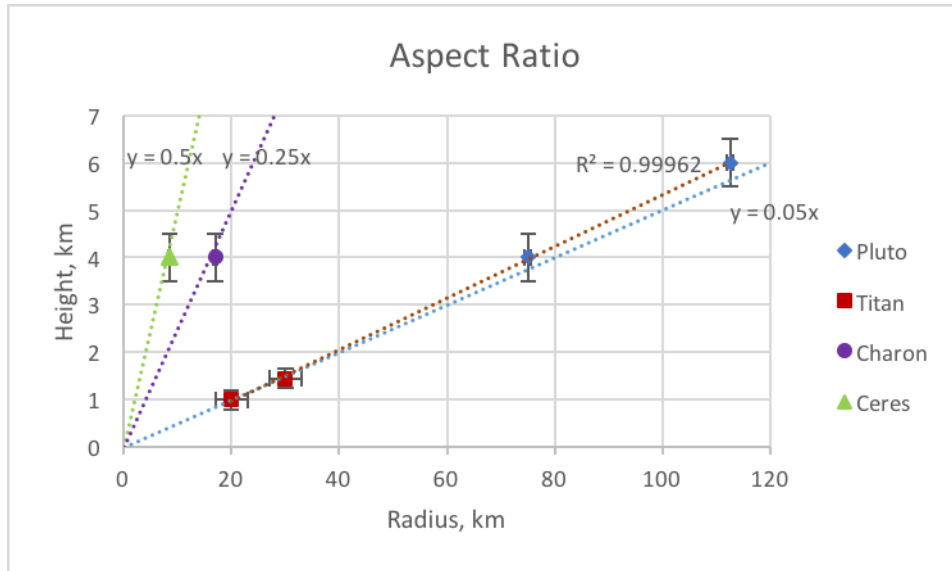


Figure 21: Plot of Figure 7 with addition of regression line between Titan and Pluto aspect ratios with R^2 value of 0.99962.

The R^2 value of the aspect ratio in Figure 21 differs by 0.00036 and 0.00236 for Figures 18 and 19, respectively. Figure 20 demonstrates that the upper bounds of viscosity would result in a morphology similar to that of volcanic domes instead of flows, but with a low aspect ratio. Additionally, the results of the similarity equations, Jeffery's equation, and Reynold's Number all support hypothesis 2; that a laminar media flow model applies to cryovolcanic flows and that Earth analogs can be used to constrain the depth, flow rate and viscosity.

Error Analysis and Discussion:

The accuracy of measurements on cryovolcanic structures varies across not only with the resolution and statistics of the spectrometers on the different spacecraft but also on the different satellites being measured and the location of the features being measured in relation to the spectrometers. The location of the feature in relation to the spectrometer is important due to the distance between them and the angle because these can affect the area per pixel in the image. The angular aperture for the spectrometer also vary from spacecraft to spacecraft and variations such as exposure time can result in variations from image to image.

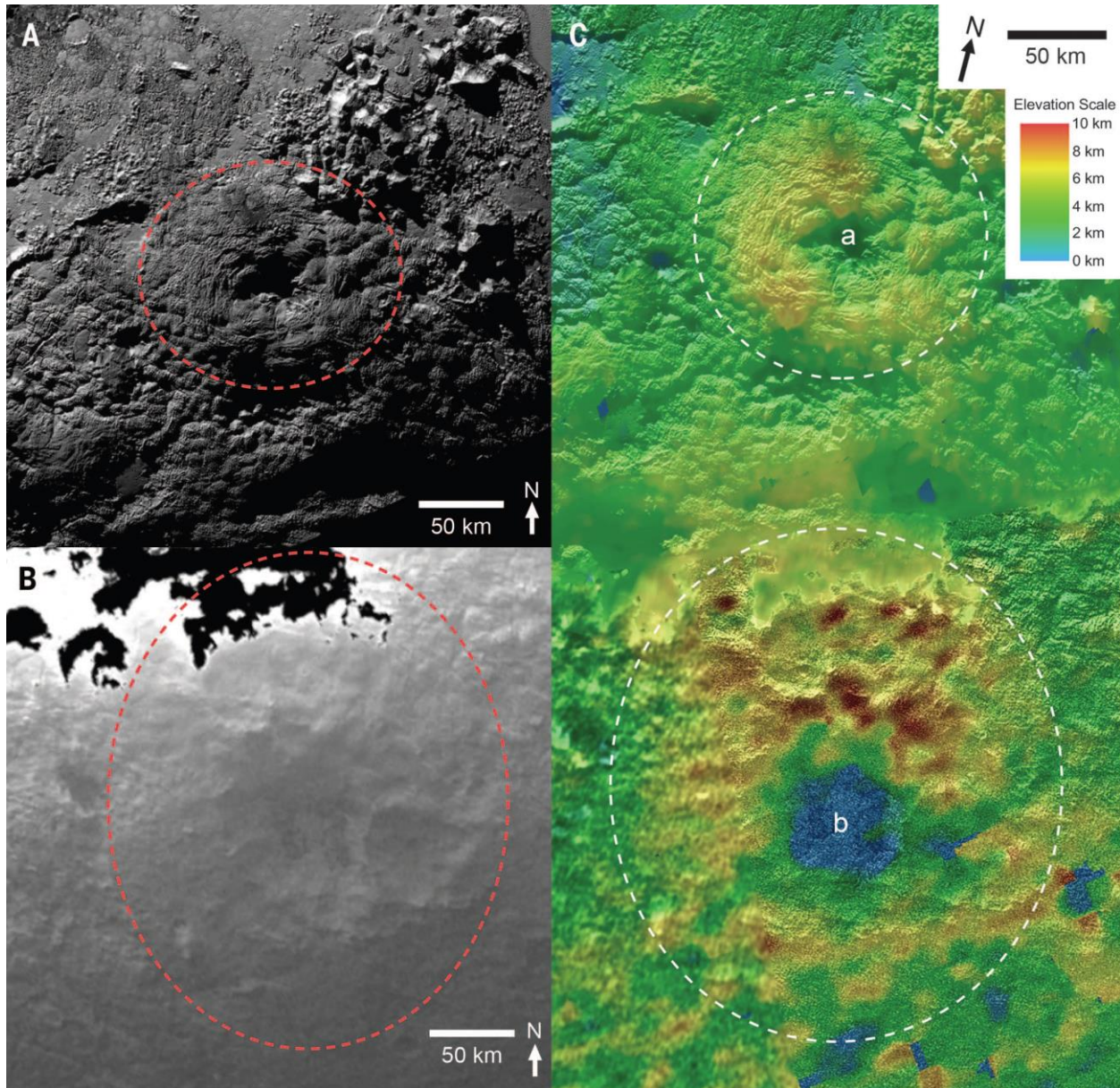


Image 2: The accuracy of imaging and thus measurements is dependent on various factors such as the distance from the surface the spacecraft is, as well as spectrometer limitations. Image from Moore and McKinnon, (2016).

Each measurement of an edifice has error not only due to the resolution of the spectrometer, but also the location and perspective the device is documenting the feature from. Additionally, the estimates on composition also contribute some error for the experiment as other important factors such as density- which is a main factor in calculating shear stress, viscosity, and Reynold's number are derived.

To conduct this research, various assumptions had to be made about the edifices and their properties. First, the edifice is a perfectly circular feature with a constant radius and constant hill slope gradient. Additionally, for the Jeffery's equation there is the assumption of a constant flow rate the does not change anywhere along the edifice and that the volume of extruded material is

evenly distributed. Thickness and viscosity are also held at constants due to the assumption of an unchanging thickness as the flow extrudes and a viscosity that is not changing with cooling. The change in viscosity with cooling would then influence the flow velocity. In reality, separate eruptions show variations in viscosity, velocity, and thickness for the same volcano. These variations exist due to compositional changes due to magma extrusion, new melt, changes in gas content, and overall volume of variations in eruption.

The calculations affected by thickness of flow, such as shear stress, Reynold's Number, and flow rate also contain uncertainty. This is due to thickness being a value that is not constant between edifices or even constant for separate eruptions from the same volcano. Thicknesses of active flows are not well documented, especially in relation to the lavas characteristics such as velocity and viscosity. This is due to the danger of surveying active lava flows and the risk of damage to equipment. As a result, numerous parameters of volcanic flows are not well constrained, including flow rate, viscosity, and viscosity change with time. Therefore, most lava flow models assume constants for values such as thickness and have a range of viscosity and flow rate to test based off of the limited data received from observed flows.

Due to flow rate and viscosity are being inversely proportional to each other figuring out the range of values for one can constrain the values of the other. The fastest observed flow of a basaltic volcano is approximately 2.8 m/s and a commonly used lower bound for lava flow models is 0.01 m/s. As a result, the range of values for velocity used was 0.01-3.0 m/s. Additionally, due to the fact that the aspect ratios of Titan and Pluto are similar the main factor that effects viscosity are gravity and density. While gravity is well constrained for each satellite, the density of each edifice is not. This is due to composition being only compared to surrounding material and actual mixture ratios not being clearly defined.

Conclusions:

With respect to aspect ratio, the dimensional characteristics of Titan and Pluto are very similar and when compared to the aspect ratio of terrestrial shield volcanoes, the similarities support these cryovolcanoes being classified as cryovolcanic shields built by flows. Previous work done on Ahuna Mons, Ceres by Ruesch et al. (2016) along with the edifices aspect ratio support it being a cryovolcanic dome. Additionally, the high aspect ratio of Kubrick Mons on Charon indicates that its morphology is not consistent with volcanoes built by flows. This supports the hypothesis that edifice dimensions can indicate differences in cryovolcanic formation and eruption style.

In addition to Titan and Pluto's cryovolcanoes being dimensionally consistent with shield volcanoes, using laminar flow constraints on Reynold's Numbers provided a range of estimates for flow velocity and viscosity. The characteristics that result in similar dimensions between the four edifices is a combination of gravity and composition. The characteristics influenced by composition and gravity also result in the size differences between the two systems. While at first taking into account gravity one would expect the satellite with the highest gravity to have the farthest runout distance it is in fact the opposite. This is due to composition effecting the flow rate and the viscosity, meaning Pluto either has a higher flow rate than Titan, a lower viscosity, or a combination of the two, while still maintaining a laminar flow. As previously stated, the high viscosity end of Figure 15 is improbable due to the results of the similarity equations and that the Jeffery's equation does not account for flow radius. However, in the case that those values are valid it is another possibility that Pluto can have a viscosity higher or equal to Titan.

This would require Pluto to have a significantly lower velocity, but as previously stated is improbably with Pluto having radii over 100 kilometers.

In regard to thickness of cryovolcanic flows, either their thickness is significantly higher than the earth average of ~10, to maintain a similar shear stress to terrestrial volcanoes (Park and Iversen, 1984). An alternative explanation is that it requires a significantly lower shear stress to form morphologically similar edifices of different material. Thickness of cryovolcanic flows can not be confirmed without observation of an erupting flow, however high flow thickness would also contribute to slower cooling rate, which could explain how cryovolcanic flows can have radii of over 100 km without solidifying at the low surface temperatures of these icy bodies.

Future studies and observations of these edifices can provide more definitive and refined insight onto cryovolcanic processes and volatile liquid behavior at low temperatures. Specifically, further refining the composition of these edifices can allow for more accurate calculations of flow characteristics such as viscosity and velocity. Furthermore, study of possible active cryovolcanism on Enceladus can provide information on changes in flow viscosity over time and cooling rates, variables which due to limited information were not available to study.

Appendix:

Equation	Variables
Dome Static Model	
$\frac{d(\sin(\phi))}{dr} + \frac{\sin(\phi)}{r} = \frac{\rho g}{\sigma t} \quad (8)$	ϕ =angular coordinate r =radius ρ =density g =gravity constant σ =tensile strength t =thickness
$\tan(\phi) = \frac{dz}{dr} \quad (9)$	ϕ =angular coordinate z =radial coordinate r =radius
$D = \frac{1}{h} \sqrt{\frac{\sigma t}{\rho g}} \quad (10)$	D =dome shape h =height σ =tensile strength t =thickness ρ =density g =gravity constant
Dome Dynamic Model	
$h(r, t) = \frac{4V}{3\pi r_0^2} \frac{1}{\left(1 + \frac{\theta}{t}\right)^{\frac{1}{4}}} \left[1 - \frac{r^2}{r_0^2} \frac{1}{\left(1 + \frac{\theta}{t}\right)^{\frac{1}{4}}} \right] \quad (11)$	$h(r, t)$ =height with respect to radius and time V =volume r_0 =initial radius t =time r =radius θ =transformation variable
$\theta(t) = \Gamma \left(1 - e^{\frac{-t}{\Gamma}} \right) \quad (12)$	$\theta(t)$ =transformation variable of time dependent viscosity Γ =timescale over which viscosity increases exponentially t =time
$v = v_0 e^{\frac{t}{\Gamma}} \quad (13)$	v =viscosity v_0 =initial bulk kinematic viscosity

		<i>t=time</i> <i>Γ=timescale over which viscosity increases exponentially</i>
$t = \left(\frac{3}{4}\right)^5 \left(\frac{\pi}{V}\right) \frac{3v_0 v_0^8}{g}$	(14)	<i>t=time constant</i> <i>V=volume</i> <i>v₀=initial bulk kinematic viscosity</i> <i>g=gravity constant</i>
$t_c \sim \frac{d^2}{\kappa}$	(15)	<i>d=dome elevation</i> <i>t_c=cooling by conduction</i> <i>κ=thermal diffusivity</i>
$t_r \sim \frac{\rho c_p d}{\sigma T^3}$	(16)	<i>ρ=density</i> <i>t_r=relaxation time</i> <i>σ=Stefan-Boltzmann constant</i> <i>d=dome elevation</i> <i>c_p=heat capacity</i> <i>T=temperature</i>
Aspect Ratio		
$\alpha = \frac{h}{r}$	(1)	<i>α=edifice slope</i> <i>h=height</i> <i>r=radius</i>
Debris Flows		
$L \sim g V^{\frac{1}{3}}$	(2)	<i>L=flow length</i> <i>g=gravity constant</i> <i>V=volume</i>
$L \sim g^{\frac{5}{6}} V^{\frac{1}{2}}$	(3)	<i>L=flow length</i> <i>g=gravity constant</i> <i>V=volume</i>
Other Equations		
$V = \pi r^2 \frac{h}{3}$	(4)	<i>V=volume</i> <i>r=radius</i> <i>h=height</i>
$PE = mgh$	(5)	<i>PE=potential energy</i> <i>m=mass</i> <i>g=gravity constant</i> <i>h=height</i>
		<i>ρ=flow density</i>

$Flow\ Shear\ Stress = \rho g d \alpha$	(6)	g =gravity constant d =flow thickness α =edifice slope
$A = \pi r^2$	(7)	A =area r =radius
Flow Equations		
$f = \left[\frac{k \rho g}{\mu Q_0} \right]^{\frac{1}{2}} h$	(17)	f =similarity value of height k =thermal diffusivity ρ =flow density g =gravity constant μ =viscosity Q_0 =flow velocity h =height
$\eta = \left[\frac{\mu}{k \rho g Q_0 t^2} \right]^{\frac{1}{4}} r$	(18)	η =similarity value of height k =thermal diffusivity ρ =flow density g =gravity constant μ =viscosity Q_0 =flow velocity t =time r =radius
$f \frac{d^2 f}{d\eta^2} + \left(\frac{df}{d\eta} \right)^2 + \frac{f}{\eta} \frac{df}{d\eta} + \frac{\eta}{2} \frac{df}{d\eta} = 0$	(19)	f =similarity value of height η =similarity value of radius
$\mu = \frac{\rho g d^2}{3V} \alpha$	(20)	μ =viscosity ρ =flow density g =gravity constant d =flow thickness V =flow velocity α =edifice slope
$Reynold's\ Number = \frac{\rho V d}{\mu}$	(21)	ρ =flow density V =flow velocity d =flow thickness μ =viscosity

I pledge on my honor that I have not given or received any unauthorized assistance or plagiarized on this assignment.
-Caroline Liegey

Bibliography

Baratoux, D., Pinet, P., Toplis, M. J., Mangold, N., Greeley, R., and Baptista, A. R. (2009). Shape, Rheology and Emplacement Times of Small Martian Shield Volcanoes. *Journal of Volcanology and Geothermal Research*, 185, 47-68.

Desch, S. J., and Neveu, M. (2016) "Differentiation and cryovolcanism on Charon: A view before and after New Horizons" School of Earth and Space Exploration, Arizona State University. 287, 175-186.

de Silva, S. (2016) "Explore Volcanoes On Venus!" Volcanoes on Venus. Oregon State University.

Diniega, S., S. E. Smrekar, S. Anderson, and E. R. Stofan (2013), The influence of temperature-dependent viscosity on lava flow dynamics, *J. Geophys. Res. Earth Surf.*, 118, 1516–1532, doi:[10.1002/jgrf.20111](https://doi.org/10.1002/jgrf.20111).

Grundy, W.M., Binzel, R.P. , (2016). Surface compositions on Pluto and Charon. 47th Lunar and Planetary Science Conference, #1737.

Kargel, J.S. (1994) "Cryovolcanism on the Icy Satellites." *Earth, Moon and Planets*.

Lopes, R. M. C.; Kirk, R. L.; Mitchell, K. L.; et al. (2013). "Cryovolcanism on Titan: New results from Cassini RADAR and VIMS". *Journal of Geophysical Research: Planets*. 118

McCord, T. B.; Sotin, C. (2005). "Ceres: Evolution and current state". *Journal of Geophysical Research: Planets*. 110 (E5): E05009. doi:10.1029/2004JE002244

McCord, T.B.; Hansen G.B., (2006). Composition of Titan's surface from Cassini VIMS. *Planetary and Space Science*, Volume 54, Issue 15, Pages 1524–1539.

Moore, J. M., Mckinnon, W. B. (2016). "The geology of Pluto and Charon through the eyes of New Horizons", *Science* 351 (6279), 1284-1293. [doi: 10.1126/science.aad7055]

Mount, C. P., and Desch, S. J. (2016) "26th Annual Lunar and Planetary Science Conference." *Earth and Planetary Science Letters* 126.4: 509.

Nichols, R. L. (1939) "Viscosity of Lava" *The Journal of Geology*, the University of Chicago Press. 290-302

Nuclear Power for Everybody, (2017). "Reynold's Number" Nuclear Engineering. Nuclear-Power.net

Oregon State University, (2017). "How fast does lava flow?" Volcano World. Oregon State University Department of Geosciences.

Park, S. and Iversen, J. D. (1984). Dynamics of lava flow: Thickness growth characteristics of steady two-dimensional flow. *Geophysics Research Letters*, 11: 641–644. doi:10.1029/GL011i007p00641

Perez-Lopez, R. (2010). "Scaling Laws of the Size-distribution of Monogenetic Volcanoes within the Michoacán-Guanajuato Volcanic Field (Mexico)." *Scaling Laws of the Size-distribution of Monogenetic Volcanoes within the Michoacán-Guanajuato Volcanic Field (Mexico)*. *Journal of Volcanology and Geothermal Research*, 201, 65-72.

- Petrovic, J.J. (2003). Review mechanical properties of ice and snow. *J. Mater. Sci.* 38, 1–6. doi: 10.1023/A:102113412803824
- Quick, L. C. Glaze, L.S.; Baloga, S.M.; Stofan, E.R. (2016), New approaches to inferences for steep-sided domes on Venus. *J. Volc. Geoth. Res.* 319, 93–105. doi: 10.1016/j.jvolgeores.2016.02.028
- Ruesch, O. *et al.*, (2016). *Science* 353, aaf4286. DOI: 10.1126/science.aaf4286
- Sanchez, L., and Shcherbakov, R. (2012). "Scaling Properties of Planetary Calderas and Terrestrial Volcanic Eruptions." *Nonlinear Processes in Geophysics*. Copernicus GmbH).
- Solar Story Network (2016). "Solar System" SolarStory.net
- Soukhovitskaya, V., Manga, M. (2005). "Martian landslides in Valles Marineris: Wet or dry?" *Icarus*, ScienceDirect.
- Spencer, J. R., Barr, A. C., and Esposito, L. W. (2009) "Enceladus: An Active Cryovolcanic Satellite." . *Enceladus: An Active Cryovolcanic Satellite*. University of Colorado
- Steigerwald, B (2016). "'Lonely Mountain' on Ceres Likely a Salty-Mud Cryovolcano." NASA.
- Stern, SA et al. (2015) "The Pluto system: Initial results from its exploration by New Horizons" *Science* 350, aad1815
- USGS (2012) "Doom Mons" International Astronomical Union (IAU) Working Group for Planetary System Nomenclature (WGPSN).
- Witze, A. (2015). "Icy volcanoes may dot Pluto's surface". *Nature News and Comment*. Nature Publishing Group. doi:10.1038/nature.2015.18756